Pure Appl. Chem., Vol. 84, No. 2, pp. 335–375, 2012.
http://dx.doi.org/10.1351/PAC-REP-11-01-11

Remote sensing in coastal water monitoring: Applications in the eastern Mediterranean Sea (IUPAC Technical Report)*

Manos Dassenakis[1,‡], Vasiliki Paraskevopoulou[1], Constantinos Cartalis[2], Nektaria Adaktilou[2], and Katerina Katsiabani[2]

[1]Department of Chemistry, Laboratory of Environmental Chemistry, University of Athens, Panepistimioupoli Zografou, GR-15771 Athens, Greece; [2]Department of Physics, Laboratory of Remote Sensing, University of Athens, Panepistimioupoli Zografou, GR-15771 Athens, Greece

Abstract: Remote sensing/satellite observation of land and oceans is a field of research that was developed during the second half of the 20th century, and its importance is widely recognised because of the amount of information it can provide to the scientific community and the general public. The outcomes of remote sensing/satellite observation can be used to address and study significant aspects of environmental concern, such as habitat destruction, environmental degradation, forest fires, oil spills, and climate change. There is continuous improvement of the methods and means of remote sensing observations in order to achieve more accurate and useful information. The main advantage is the possibility of observing large areas, and the main disadvantage is that it can observe only the water and land surface. The present paper is an effort to review the technologies used in remote sensing and the general applications in a comprehensive manner addressed to scientists who do not specialize in this area of research. Furthermore, this paper reviews case studies/applications in the Mediterranean Sea, an area affected by various polluting activities (industrial cities, agriculture, shipping, etc.) that should be continuously monitored so that the coastal countries are able to successfully manage this sensitive environment.

Keywords: chlorophyll; coastal management; eutrophication; IUPAC Chemistry and the Environment Division; Mediterranean Sea; oil spills; remote sensing.

CONTENTS

*Sponsoring body: IUPAC Chemistry and the Environment Division: see more details on page 373.
‡Corresponding author

1. INTRODUCTION

Coastal zones are important, sensitive ecological systems and are also significant from an economic point of view as they are used for tourism, fishing, aquaculture, and recreation. Many times, their significance is ignored and they are overexploited or subjected to intense environmental pressures. Large loads of land-based pollutants from industrial, urban, and agricultural activities are disposed to coastal areas. Physical, chemical, biological, or thermal pollution can cause adverse effects to the marine environment, ecological damage, and even pose dangers to public health.

Therefore, the necessity of environmental monitoring is undisputed. There is a simultaneous need for both large-scale observation and monitoring of ocean processes as well as small-scale monitoring campaigns, e.g., for enclosed polluted gulfs, specific river catchments, etc.

Remote sensing techniques have been utilised with various types of sensors and for various applications in environmental purposes since the early 1960s. Weather monitoring and forecasting was one of the first applications of satellite remote sensing, but it was soon apparent that satellites could also be used for detailed mapping of the land surface and for the monitoring of the oceans.

The importance of marine processes in the global climate system has been stressed repeatedly, and therefore the main advantage of satellite remote sensing of the oceans is the fact that it provides large-scale and simultaneous monitoring of entire basins. At the same time, it can also be used in smaller scales and coastal areas that are subject to intense environmental pressures, but these applications have not been developed enough because of the inadequate resolution of the satellites' sensors in small areas.

On the other hand, only a few chemical applications and/or pollutants are detectable in the marine environment by remote sensing techniques. These are chlorophyll (chl)-like pigments, suspended particulate material, and oil. In the case of oil spills, only high concentrations on the sea surface from large-scale accidents are mostly detected and monitored and not smaller accidental discharges. Therefore, there should be some effort to combine the large-scale monitoring of remote sensing with targeted in situ observations so that their results are complementary to one another with a final aim to ensure effective protection of the marine environment.

The present paper aims to review remote sensing technologies and applications. In Sections 1–5, the sensor technologies and general applications are reviewed. In Sections 6–10, there is detailed mention of remote sensing marine applications and case studies. An effort was made to focus on the Mediterranean Sea including eastern Mediterranean case studies even though there is limited work in this marine area. Large-scale case studies in the world's oceans (Atlantic, Pacific, etc.) are beyond the scope of this paper and were not reviewed.

2. OVERVIEW OF REMOTE SENSING TECHNOLOGY: BASIC PRINCIPLES AND SATELLITE CHARACTERISTICS [1]

Remote sensing is the science of acquiring information about the Earth's surface without actually being in contact with it. This is done by sensing and recording reflected or emitted energy and processing, analyzing, and applying that information. The process generally involves an interaction between incident radiation and the targets of interest. This is exemplified by the use of imaging systems. However, there are cases in which remote sensing also involves the sensing of emitted energy and the use of non-imaging sensors.

Figure 1 schematically presents the basic requirements for remote sensing applications. The energy source or illumination medium (A) provides electromagnetic energy to the target of interest. The regions of the electromagnetic spectrum mostly used for remote sensing applications are: UV (10–400 nm), visible (400–700 nm), IR (0.7–100 μm) distinguished in reflected (0.7–3 μm) and thermal IR (TIR) (3–100 μm), and more recently the microwave region (1 mm to 1 m). The energy traveling from the light source to the target and from the target to the sensors interacts with the Earth's atmosphere (B) and is subject to scattering and absorption. The electromagnetic spectrum regions mentioned above are not subject to significant absorption—they are called "atmospheric windows" and are thus useful for remote sensing.

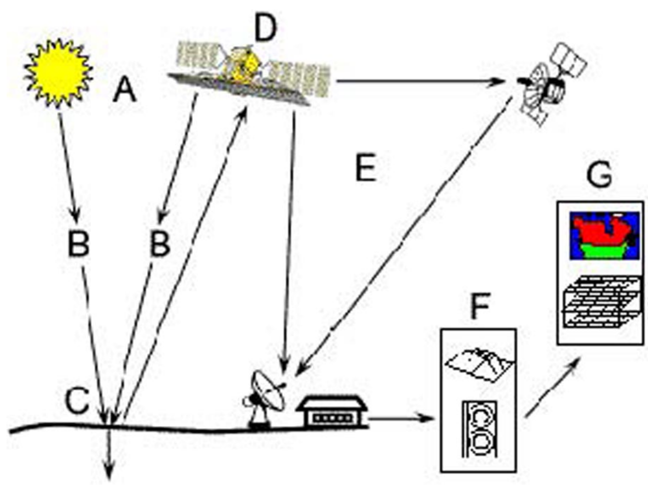

Fig. 1 Schematical representation of remote sensing operating principle[1], © CCRS/CCT.

The interaction between energy and target (C) depends on the properties of both the target and the radiation. There are three forms of interaction that can take place when energy strikes, or is incident upon a target surface. Absorption (A) occurs when radiation (energy) is absorbed into a target, transmission (T) occurs when radiation passes through it, and reflection (R) occurs when radiation "bounces" off the target and is redirected. In remote sensing, we are most interested in measuring the radiation reflected from targets.

After the energy has been scattered by or emitted from the target, a remote sensor collects and records the electromagnetic radiation (D). Remote sensing systems, which measure energy that is naturally available, are called passive sensors. The sun provides this naturally available energy. The sun's energy is either reflected (visible wavelengths), or absorbed and then reemitted (TIR wavelengths). Passive sensors can only be used when the naturally occurring energy is available, which is during the day for reflected energy and both day and night for emitted energy (TIR). Active sensors, on the other hand, provide their own energy source for illumination. The sensor emits radiation, which is directed toward the target. The radiation reflected from that target is detected and measured by the sensor. Advantages for active sensors include the ability to obtain measurements anytime, regardless of the time of day or season. Active sensors can be used for examining wavelengths that are not sufficiently provided by the sun, such as microwaves, or to better control the way a target is illuminated. However, active systems require the generation of a fairly large amount of energy to adequately illuminate targets.

Active microwave sensors are generally divided into two distinct categories: imaging and non-imaging. The most common form of imaging active microwave sensors is RADAR. **RADAR** is an acronym for **RA**dio **D**etection **A**nd **R**anging, which essentially characterizes the function and operation of a radar sensor. The sensor transmits a microwave (radio) signal toward the target and detects the back-scattered portion of the signal. The strength of the back-scattered signal is measured to discriminate between different targets, and the time delay between the transmitted and reflected signals determines the distance (or range) to the target. Some examples of active sensors are the non-imaging altimeters and scatterometers and the imaging SLAR (side-looking airborne radar) and SAR (synthetic aperture radar).

The energy recorded by any sensor has to be transmitted, often in electronic form, to a receiving/processing station where the data are processed into an image (hard copy and/or digital) (E). The processed image is interpreted, visually and/or digitally or electronically, to extract information about the target that was illuminated (F). The final product (G) of the remote sensing process is achieved when we apply the information we have been able to extract from the imagery about the target in order to better understand it, reveal some new information, or assist in solving a particular problem.

Although ground-based and aircraft platforms may also be used, satellites provide most of the remote sensing imagery used today. Satellites have several unique characteristics, which make them particularly useful for remote sensing of the Earth's surface. The main satellite characteristics are discussed below.

The path followed by a satellite is referred to as its orbit. Satellite orbits are matched to the capability and objective of the sensor(s) they carry. Orbit selection can vary in terms of altitude (their height above the Earth's surface) and their orientation and rotation relative to the Earth. The geostationary satellites rotate with the Earth continuously over a specific area, like the satellites used for weather applications and communications. Other satellites follow near-polar orbits, which means that they are ascending toward the North Pole and then descend toward the South Pole, thus achieving full coverage of the Earth's surface due to its rotation.

The *spatial resolution* of the sensor determines the detail discernible in an image and refers to the size of the smallest possible feature that can be detected. The area on the ground "seen" by a satellite is called the resolution cell and determines a sensor's maximum spatial resolution.

Most remote sensing images are composed of a matrix of picture elements, or pixels, which are the smallest units of an image. Image pixels are normally square and represent a certain area on an image. If a sensor has a spatial resolution of 20 m and an image from that sensor is displayed at full resolution, each pixel represents an area of 20×20 m on the ground. In this case, the pixel size and resolution are the same. However, it is possible to display an image with a pixel size different than the resolution.

Spectral resolution describes the ability of a sensor to define fine wavelength intervals. The finer the spectral resolution, the narrower the wavelength range is for a particular channel or band. Many remote sensing systems record energy over several separate wavelength ranges at various spectral resolutions. These are referred to as multispectral sensors. Advanced multispectral sensors, called hyperspectral sensors, detect hundreds of very narrow spectral bands throughout the visible, near-IR, and mid-IR portions of the electromagnetic spectrum. Their very high spectral resolution facilitates fine discrimination between different targets based on their spectral response in each of the narrow bands.

The *radiometric resolution* of an imaging system describes its ability to discriminate very slight differences in energy. The finer the radiometric resolution of a sensor, the more sensitive it is to detecting small differences in reflected or emitted energy.

In addition to spatial, spectral, and radiometric resolution, the concept of *temporal resolution* is also important. The revisit period refers to the length of time it takes for a satellite to complete one entire orbit cycle. The revisit period of a satellite sensor is usually several days. Therefore, the absolute temporal resolution of a remote sensing system to image the exact same area at the same viewing angle a second time is equal to this period. However, because of some degree of overlap in the imaging swaths of adjacent orbits for most satellites and the increase in this overlap with increasing latitude, some areas of the Earth tend to be re-imaged more frequently. Also, some satellite systems are able to point their sensors to image the same area between different satellite passes separated by periods from one to five days. Thus, the actual temporal resolution of a sensor depends on a variety of factors, including the satellite/sensor capabilities, the swath overlap, and latitude. The ability to collect imagery of the same area of the Earth's surface at different periods of time is one of the most important elements for applying remote sensing data.

3. REMOTE SENSING APPLICATIONS: WEATHER SATELLITES—METEOROLOGY [1]

Weather monitoring and forecasting was one of the first civilian (as opposed to military) applications of satellite remote sensing. Today, several countries operate weather, or meteorological, satellites to monitor weather conditions around the globe. Generally speaking, these satellites use sensors that have fairly coarse spatial resolution (when compared to systems for observing land) and provide large areal coverage. Their temporal resolutions are quite high, providing frequent observations of the Earth's surface, atmospheric moisture, and cloud cover, which allows for near-continuous monitoring of global weather conditions, and hence, forecasting. Some satellites used for weather applications since the 1960s were the following:

- NASA (U.S. National Aeronautics and Space Administration) in collaboration with NOAA (U.S. National Oceanic and Atmospheric Administration) launched the ATS series (Applications Technology Satellites) and later the GOES (Geostationary Operational Environmental System) which are geostationary satellites covering one third of the Earth, namely, North and South America, the Pacific Ocean, and most of the Atlantic Ocean. The sensors of these satellites operate in the vis/IR parts of the electromagnetic spectrum and they detect cloud, pollution, haze, storms, fog, ice clouds, forest fires, volcanoes, moisture, rain fall, and sea surface temperature (SST).
- Another NASA-NOAA satellite series are the AVHRR (Advanced Very High Resolution Radiometer) satellites with near-polar orbits providing global coverage of cloud, snow, ice, water, vegetation, SST, volcanoes, forest fires, and moisture with observations in the vis/IR and TIR spectrum.
- Some more weather satellites are operated by the United States and the DMSP (Defense Meteorological Satellite Program). These are near-polar orbiting satellites with two broad wavelength bands (visible to near-IR and TIR band). An interesting feature of the sensor is its ability to acquire visible band night-time imagery under very low illumination conditions, and thus it can acquire striking images of the Earth showing the night-time lights of large urban centres.
- There are several other meteorological satellites in orbit, launched and operated by other countries, or groups of countries. These include Japan, with the GMS satellite series, and the consortium of European communities, with the Meteosat satellites. Both are geostationary satellites situated above the Equator over Japan and Europe, respectively.

4. REMOTE SENSING APPLICATIONS: LAND OBSERVATION SATELLITES [1]

Although many of the weather satellite systems (such as those described in the previous section) are also used for monitoring the Earth's surface, they are not optimized for detailed mapping of the land surface. NASA and NOAA operated since 1972 the Landsat series of satellites which later became commercialised and provide data to civilian and applications users. The orbits are near-polar, and the sensors multispectral scanner (MSS) and thematic mapper (TM) operating in the vis/IR and TIR spectrum can record images and provide information on soil-vegetation, altimetry, mineral rock types, cultural features and moisture that can be used for resource management, cultural and thermal mapping, environmental monitoring, and detection of change (e.g., monitoring forest clear-cutting).

SPOT (Système Pour l'Observation de la Terre) is a series of Earth observation imaging satellites designed and launched by CNES (Centre National d'Études Spatiales) of France, with support from Sweden and Belgium. The HRV (high resolution visible) sensors of SPOT allow applications requiring fine spatial detail (such as urban mapping) to be addressed. Furthermore, SPOT is useful for applications that require frequent monitoring, e.g., agriculture and forestry.

The Indian Remote Sensing (IRS) satellite series combines features from both the Landsat MSS/TM sensors and the SPOT HRV sensor, thus providing high-resolution data useful for urban planning, mapping applications, vegetation discrimination, and natural resource planning.

Currently, there are several satellites used for land observation purposes launched by national space agencies (e.g., United States, Canada, China, Japan, Italy, Brazil, Germany, etc.) as well as regional or international agencies (European Space Agency, ESA) [2].

The usefulness of satellite remote sensing for *land monitoring applications* can be summarised as follows. Satellite and airborne images are used as mapping tools to monitor crop type, health, yield estimation, soil characteristics, soil management, and farming practices. Multispectral sensors (UV to IR) provide information on the phenology (growth), stage type, and crop health; radar is sensitive to the structure, alignment, and moisture content of the crop and thus can provide complementary information to the optical data. Images of crops can be obtained throughout the growing season to not only detect problems, but also to monitor the success of the treatment.

Forestry applications of remote sensing include reconnaissance mapping (forest cover updating and measuring biophysical properties of forest stands), forest cover-type discrimination, commercial forestry inventory and mapping applications for companies and resource management agencies, and, finally, environmental monitoring for conservation authorities, which refers to information on deforestation (rainforest, mangrove colonies), species inventory, watershed protection, coastal protection (mangrove forests), and forest health. Large-scale species identification can be performed with multispectral, hyperspectral, or air-photo data, while small-scale cover-type delineation can be performed by radar or multispectral data interpretation. Remote sensing can be used to detect and monitor forest fires and the regrowth following a fire. NOAA AVHRR thermal data and GOES meteorological data can be used to delineate active fires and remaining "hot spots" when optical sensors (photo–video) are hindered by smoke, haze, and/or darkness.

Geological applications of remote sensing include: surficial deposit/bedrock, lithological and structural mapping, sand and gravel (aggregate) exploration/exploitation, mineral exploration, hydrocarbon exploration, environmental geology, geobotany, sedimentation mapping and monitoring, event mapping and monitoring, geohazard mapping, and planetary mapping. Multispectral data can provide information on lithology or rock composition based on spectral reflectance. Radar provides an expression of surface topography and roughness, and thus is extremely valuable, especially when integrated with another data source to provide detailed relief. Remote sensing gives the overview required to (1) construct regional unit maps, useful for small-scale analyses, and planning field traverses to sample and verify various units for detailed mapping; and (2) understand the spatial distribution and surface relationships between the geological units.

Examples of *hydrological applications* include wetlands mapping and monitoring, soil moisture estimation, snow pack monitoring/delineation of extent, measuring snow thickness, determining snow-water equivalent, river and lake ice monitoring, flood mapping and monitoring, glacier dynamics monitoring (surges, ablation), river/delta change detection, drainage basin mapping and watershed modeling, irrigation canal leakage detection, and irrigation scheduling. Passive and active radar sensors have brought a new dimension to hydrological studies with its active sensing capabilities, allowing the time window of image acquisition to include inclement weather conditions or seasonal or diurnal darkness. Also, coarse resolution optical sensors such as NOAA's AVHRR are used to provide an excellent overview of pack ice extent if atmospheric conditions are optimal (resolution = 1 km).

Land use applications of remote sensing include the following: natural resource management, wildlife habitat protection, baseline mapping for geographical information system (GIS) input, urban expansion/encroachment, routing and logistics planning for seismic/exploration/resource extraction activities, damage delineation (tornadoes, flooding, volcanic, seismic, fire), legal boundaries for tax and property evaluation, and target detection/identification of landing strips, roads, clearings, bridges, and land/water interface [1].

The main *mapping applications* of remote sensing are: (a) planimetry (identification and geolocation of basic land cover, e.g., forest, marsh, drainage, and anthropogenic features, e.g., urban infrastructure, transportation networks in the *x*, *y* plane with the provided information to be used for large-scale applications such as surban mapping, facilities management, military reconnaissance, and general landscape information); (b) digital elevation models (DEMs); and (c) baseline thematic mapping/topographic mapping. Finally, there is a growing demand for digital databases of topographic and thematic information to facilitate data integration and efficient updating of other spatially oriented data.

All of the above applications are combined with GIS.

5. REMOTE SENSING APPLICATIONS: MARINE OBSERVATION SATELLITES/SENSORS

The Earth's oceans cover more than two-thirds of the Earth's surface and play an important role in the global climate system. They also contain an abundance of living organisms and natural resources that are susceptible to pollution and other man-induced hazards. The meteorological and land observation satellites/sensors that have already been discussed in Section 3 can also be used for monitoring the oceans, but there are other satellite/sensor systems that have been designed specifically for this purpose [1].

The Nimbus-7 satellite, launched in 1978 and placed in a sun-synchronous, near-polar orbit, carried the first sensor, the coastal zone colour scanner (CZCS), specifically intended for monitoring the Earth's oceans and water bodies. The primary objective of this sensor was to observe ocean colour and temperature, particularly in coastal zones, with sufficient spatial and spectral resolution to detect pollutants in the upper levels of the ocean and to determine the nature of materials suspended in the water column. The repeat cycle of the satellite allowed for global coverage every six days. The CZCS sensor consisted of six spectral bands in the visible, near-IR, and thermal portions of the spectrum. Bands 1 to 4 of the CZCS sensor (0.43–0.68 μm) were very narrow and optimized to allow detailed discrimination of differences in water reflectance owing to phytoplankton concentrations and other suspended particulates in the water. In addition to detecting surface vegetation on the water, band 5 was used to discriminate water from land prior to processing the other bands of information, and finally band 6 was used for monitoring SST. The CZCS sensor ceased operation in 1986 [1].

The first marine observation satellite (MOS-1) was launched by Japan in February 1987 and was followed by its successor, MOS-1b, in February 1990. These satellites carried three different sensors: a four-channel multispectral electronic self-scanning radiometer (MESSR), a four-channel visible and thermal infrared radiometer (VTIR), and a two-channel microwave scanning radiometer (MSR). The MESSR bands are quite similar in spectral range to the Landsat MSS sensor and are thus useful for land applications in addition to observations of marine environments [1].

The SeaWiFS (sea-viewing wide field-of-view sensor) on board the SeaStar spacecraft is an advanced sensor designed for ocean monitoring. It consists of eight spectral bands of very narrow wavelength ranges tailored for very specific detection and monitoring of various ocean phenomena including: ocean primary production and phytoplankton processes, ocean influences on climate processes (heat storage and aerosol formation), and monitoring of the cycles of carbon, sulfur, and nitrogen [1]. A limitation to the exploitation of SeaWiFS is that the instrument is operated as a commercial venture with research use purchased by NASA. Operational and some near-real-time applications cannot be supported through NASA and data must be purchased from Orbview (Orbital Sciences Corporation) [3].

The first of a next generation of ocean colour instruments, the moderate resolution imaging spectroradiometer (MODIS), was launched on 18 December 1999 on-board the NASA "Terra" satellite.

MODIS represents a further leap in capability compared to SeaWiFS with more wavebands, higher signal-to-noise ratio, more complex on-board calibration, and the capability of simultaneous observation of ocean colour and SST. Further instrument launches were planned, including MODIS on “Aqua” platform (2002). This will ensure continuity of ocean colour data, and will provide two observations per day (because Terra and Aqua will pass overhead at 10:30 and 14:30 h local time, respectively). MODIS broadcasts continuously, signals can be recorded by anyone with an appropriate receiver and therefore can be used without any commercial restrictions [3,4].

The MERIS imaging multispectral radiometer (vis/IR) was launched on ESA’s Envisat platform in 2002. Its main objective is to monitor ocean colour, but atmospheric and land applications are also carried out [5–7].

The NASA Aquarius project is a focused satellite mission to measure global sea surface salinity. After its planned 2010 launch, it will provide the global view of salinity variability needed for climate studies. The objectives of this mission are to produce global salinity maps at 0.2 psu accuracy on a monthly basis at 100-km resolution (1 psu = 1 $g \cdot kg^{-1}$ salt concentration in seawater) and measure the seasonal and year-to-year variations of salinity, as well as the global annual mean [8].

The ocean-observing systems/sensors mentioned in the above sections are important for global and regional-scale monitoring of ocean pollution and health, and assist scientists in understanding the influence and impact of the oceans on the global climate system. In the following sections, there will be mention of oceans and coastal applications, the necessary validation and comparison of remote sensing to in situ data and specific case studies with focus on the Mediterranean Sea.

6. REMOTE SENSING MONITORING OF OCEAN FEATURES

Satellite thermal images, such as those obtained by AVHRR-SST have been used in order to define the time and space scales of surface temperature distributions. Apart from the use of SST data to assess climate change, the temperature distributions are related to the upper thermocline circulation. For this purpose, the satellite images are compared with conductivity–temperature–depth (CTD) casts and acoustic Doppler current profiler (ADCP) measurements during oceanographic cruises. The objectives of this integrated analysis are to provide knowledge on basin-scale circulation as well as to monitor phenomena of smaller scales, such as eddies and local currents [9–14]. Furthermore, altimeter satellite data (ERS) have been compared with buoy observations to determine not only water circulation but also sea-level statistics [15]. Some recent applications of remote sensing data in physical oceanography in the Mediterranean and Black Sea basins will be briefly presented.

An SST study of the Black Sea was carried out in order to investigate seasonal and interannual variability during the period from November 1981 to December 2000. Night-time weekly multichannel sea surface temperature (MCSST) data set based on NOAA AVHRR measurements (with spatial and temperature resolution of about 18 km and 0.1 °C) were used. The SST satellite fields averaged for the central months of four hydrological seasons (February, May, August, and November) were calculated and compared with the corresponding climatic SST fields based on in situ measurements. It turned out that the winter weekly mean SST minima fell on 1985, 1987, 1992, and 1993, SST maxima on 1984, 1988, 1995, and 1999. Since 1994, winters were relatively warm. Most of the marked anomalies of the summer and winter SSTs as well as the greatest seasonal amplitudes of SST (in 1987, 1992, and 1998) occurred either during the El Niño global events or some months later. An increasing trend of the Black Sea mean SST of about 0.09 °C per year over the period of consideration was revealed, the western deep-sea region getting warmer more slowly (about 0.08 °C per year) as compared with the eastern one (about 0.11 °C per year). In the first half of the period (1982–1991), the trends of the yearly and seasonally mean (besides the summer-averaged) SSTs were considerably less than in the second one (1992–2000); the summer-averaged SST trend was approximately the same in both of the subperiods [9].

A 10-year data set of AVHRR-SST with 18-km space resolution and weekly frequency was used to study the seasonal and inter-annual variability of the eastern Mediterranean Sea surface field. Three main objectives were addressed. The first was to define the time and space scales of the surface temperature distributions. The second objective was to relate the SST features to the upper thermocline circulation, and the third was to compare these features with the observational evidence of the Physical Oceanography of the Eastern Mediterranean (POEM) Program [10,11].

The time analysis revealed the presence of a strong seasonal signal characterized by two main seasonal extremes, winter and summer. The space analysis shows that the dominant scale is the sub-basin scale and the sub-basin gyres are very well resolved, allowing the identification of permanent and semi-permanent structures. The results for the two further objectives can be summarized together. The seasonal and monthly SST distributions are strongly correlated with the dynamical structure of the basin upper thermocline circulation. A direct comparison of the September 1987 SST pattern with the corresponding surface temperature map of the POEM-87 survey proves this correlation quantitatively. Furthermore, comparison of the SST monthly climatologies with the POEM circulation scheme showed that all the major currents and the sub-basin gyres were also found consistent with the patterns dictated by the remote sensing data (Fig. 2) [10,11].

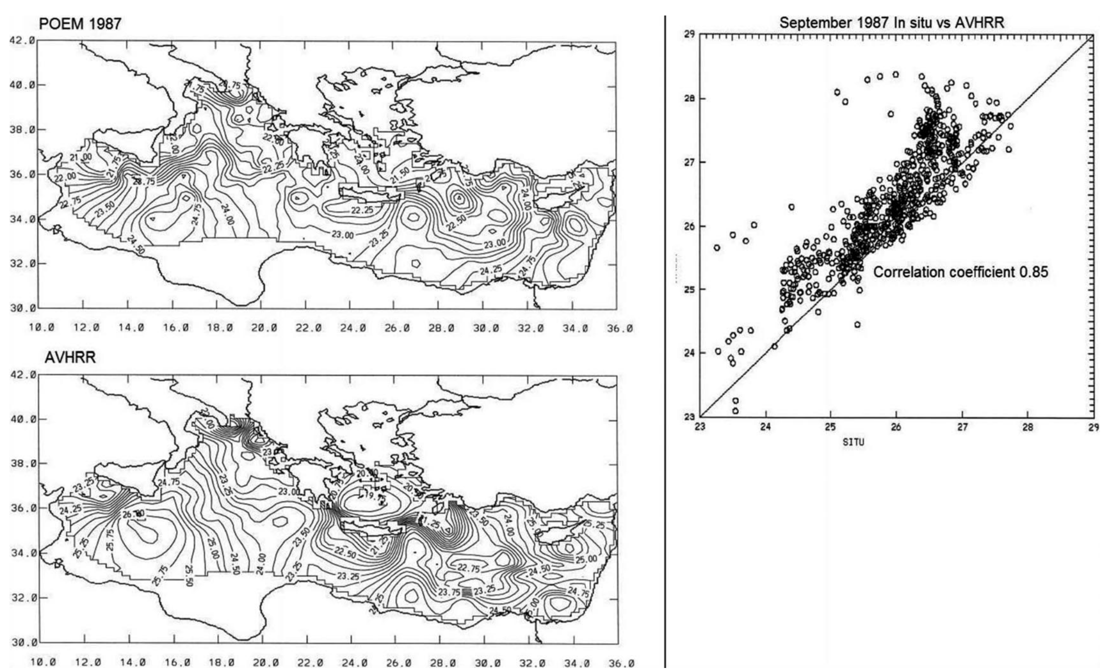

Fig. 2 SST field of September 1987. Left: POEM data above, AVHRR data below. Right: correlation of the two data sets (adapted from ref. [10]).

A study of satellite and in situ data for the eastern basin of the Mediterranean Sea was undertaken in order to verify the historically proposed Atlantic water (AW) circulation schemes. The study included detailed analysis of over 1000 daily and weekly composite images spanning the period 1996–2000, and of monthly composite images available since 1985. Whenever in situ observations were available, they were compared with the satellite thermal signatures and it was shown that both were consistent. The results of this study confirmed that AW circulates counterclockwise in the eastern basin. However, the

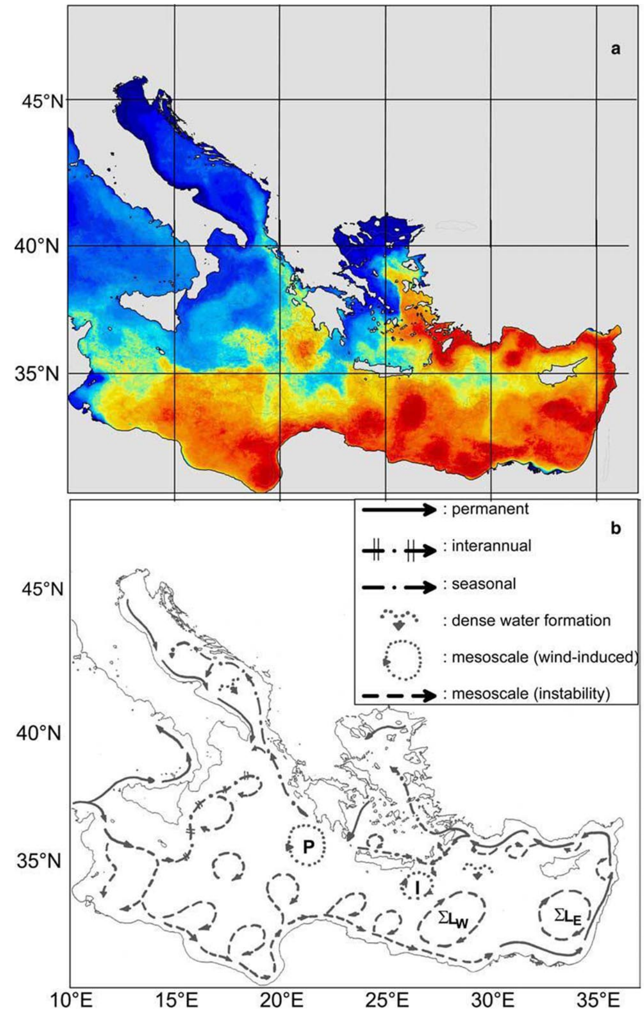

Fig. 3 The eastern basin of the Mediterranean Sea in January 1998 (SST, a), and the remote sensing surface circulation scheme (b) [12].

historical schemes represent a broad flow while this study showed that the circulation is essentially constrained along slope, being markedly unstable and generating mesoscale eddies (Fig. 3) [12].

In another study, seven years of combined maps of TOPEX/Poseidon (T/P) and ERS-1/2 altimeter data were used to describe the surface circulation variability in the Mediterranean Sea. The longer study period (1993–1999) and the merging of T/P and ERS-1/2 altimeter data allowed observation with a good accuracy the major changes that occurred in the Mediterranean Sea and, in particular, at basin and sub-basin scales. First, important interannual signals were found in the Ionian basin where the cyclonic circulation has clearly intensified since 1997. In the Levantine basin, although the Ierapetra eddy exhibits a clear seasonal cycle, it is not always present during the observation period. Secondly, the seasonal cycle of the Alboran gyres was confirmed. Moreover, these gyres and the Ierapetra eddy constitute the most intense signals of the Mediterranean Sea variability (Fig. 4). Finally, this descriptive study illustrated the need to continue monitoring the surface circulation in order to better understand the dynamics of the Mediterranean Sea [13].

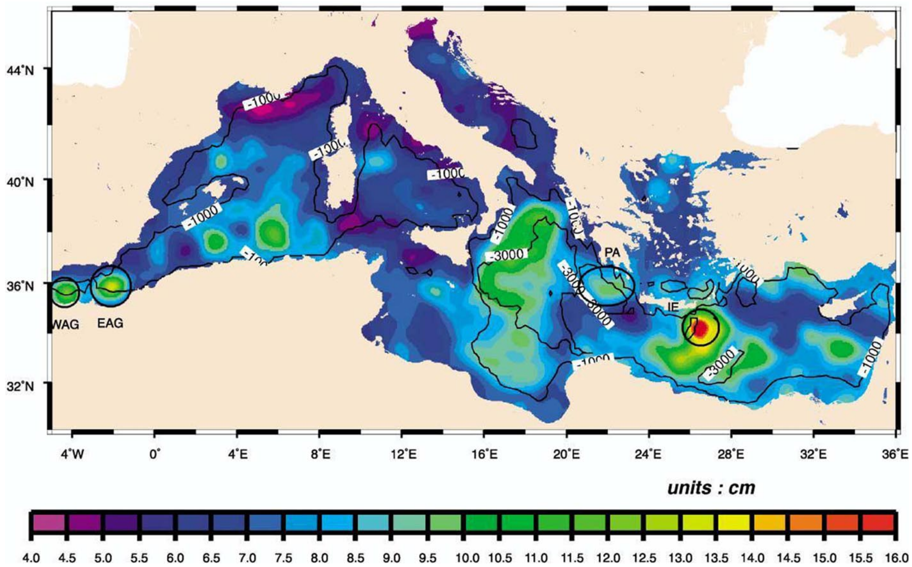

Fig. 4 The variability of SLA from combined maps of T/P and ERS-1/2 (1993–1999). Units are in cm. WA/EAG: western/eastern Alboran gyres; PE: Pelops anticyclone, IE: Ierapetra eddy [13].

Through the analysis of satellite thermal images, mesoscale anticyclonic eddies have been observed to recurrently drift along the northwestern Mediterranean coasts and the Algerian basin [14–16]. In one case, a group of anticyclonic structures were tracked from the Gulf of Lions to the Catalan shelf by analysis of SST images, and at the same time one of the eddy-like features was also intensely surveyed by means of in situ CTD casts and repeated fast surveys with oscillating CTD and ADCP measurements. It was found that the passage of the eddy modified the local flow, involving advection and subduction of surrounding waters (Fig. 5) [16].

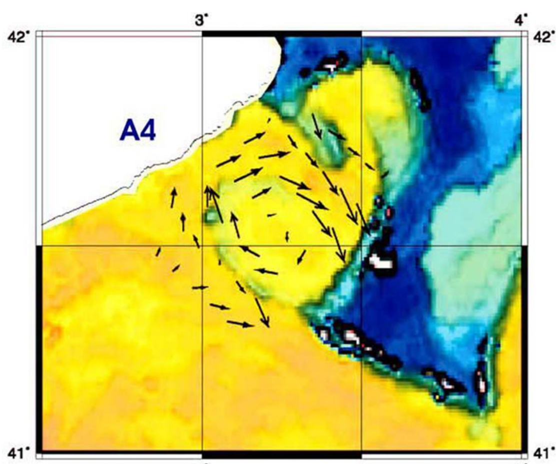

Fig. 5 SST image of 26 September. The ADCP velocity field is superimposed to the satellite image [16].

7. REMOTE SENSING MONITORING OF OCEAN COLOUR (PRIMARY PRODUCTION—CHLOROPHYLL)

The term "ocean colour" is used to indicate the visible light spectrum as observed at the sea surface, which is related, by the processes of absorption and scattering, to the concentration of water constituents, specifically chl-like pigments from phytoplankton (microscopic unicelluar algae) as well as suspended sediments, degrading organic materials, and other particulate or dissolved substances. The retrieval of environmental parameters depends on modeling the relationship between water optical properties and concentration of water constituents [17]. In this section, the quantification of oceanic phytoplankton (primary production) through satellite remote sensing of sea surface colour will be discussed in detail.

Remote sensing measurements of sea surface colour and temperature, as mentioned above, have been historically conducted by means of low-resolution (pixels of the order of 1 km) data collected in the vis/IR and TIR spectral region. Optical remote sensing allows monitoring the space and time heterogeneity of phytoplankton growth in marginal and enclosed seas, a factor critical to understanding their ecosystem dynamics [17,18].

Studies concerning sea surface optical properties relied primarily on historical data generated by CZCS, which was launched in the fall of 1978. The available data from CZCS, even though they were characterized by limited statistical coverage (owing to the low number and irregular time spacing of individual images), show consistent patterns in line with the characteristics of the European basins. In general, the same kind of large-scale colour patterns were recurrent on a regional and seasonal basis, in different years [17].

In the Mediterranean region, in particular, the ocean colour data provide indications on a number of processes owing to biological, geochemical, and physical interactions—in particular, those related to the environmental impact of coastal and river runoff, coupled with water circulation patterns. The quasi-permanent surface features of the basin are exemplified in the composite CZCS image of Fig. 6, which shows the mean annual patterns of water constituents for the period 1979–1985. The original data (2373 individual images) were processed to derive chl-like pigment concentration. The basin presents

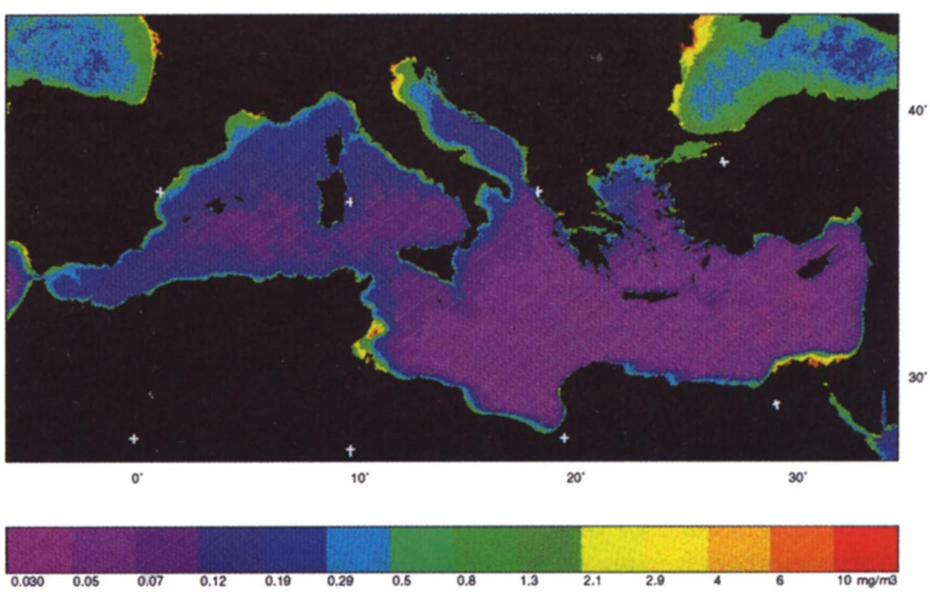

Fig. 6 Composite CZCS image of the Mediterranean basin. This image highlights the differences between Mediterranean sub-basins, the oligotrophic waters of the open sea, and the mesotrophic waters of coastal areas [17].

relatively clear, oligotrophic waters in the pelagic region, where the signal, owing to planktonic pigments, is minimum. Oligotrophic conditions are most persistent, over the annual cycle, in the eastern rather than in the western Mediterranean. Accordingly, seasonal variations were most pronounced in the western rather than in the eastern Mediterranean [17].

On the other hand, the basin presents highly dynamic, mesotrophic, at times even eutrophic, subbasins and near-coastal areas. Not surprisingly, therefore, the Mediterranean CZCS data set suggests several points of particular interest for the study of the coastal domain. Major rivers such as the Po, Rhone, Ebro (and the Nile, up to a point) or the Danube, Dnestr, and Dnepr in the Black Sea area, have distinct plumes interacting with the marine environment. Within the range of the plumes (as with coastal runoff in general), it is often impossible for the CZCS to distinguish the signature of biogenic pigments from that of the total load of dissolved and suspended materials present in the water. However, the observation of such features provides important clues on coastal frontal dynamics and potential correlations with nutrient enrichment, sediment transport, and pollution sources. An example of coastal interactions because of fluvial runoff in the northern Adriatic Sea is shown in the CZCS image of Fig. 7. Note the plume originated by the Po River (4 July 1980). The environmental characteristics of the Gulf of Venice appear to be dominated by waters of fluvial origin [17].

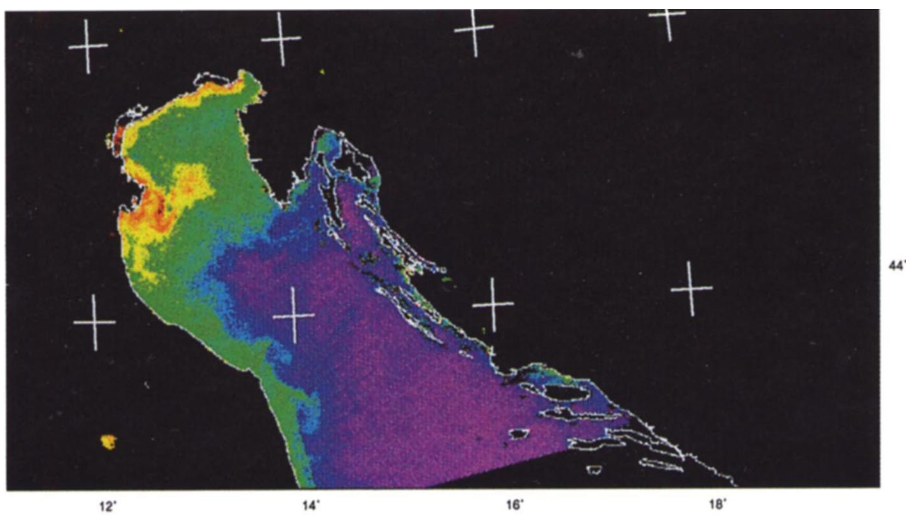

Fig. 7 Coastal features due to coastal and fluvial runoff in the northern Adriatic Sea [17].

In Fig. 8, the Nile River plume is shown instead, as it appeared to the CZCS on 25 November 1981. The coastal black rim highlights shallow waters with very high sediment load. The western portion of the plume is seen interacting with coastal currents. The connection between the eastern portion of the plume and a series of coastal filaments can be seen. In the land portion, the vegetated area of the Nile River delta, and in part the major branches of the river itself, are marked by darker tones [17].

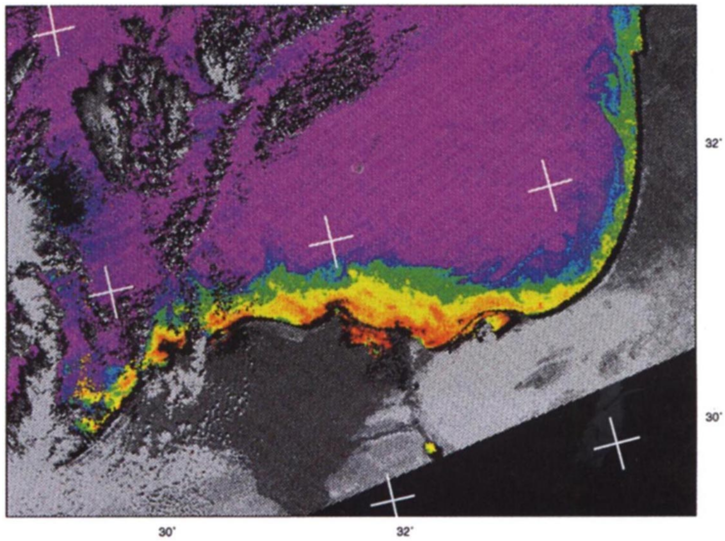

Fig. 8 The Nile River plume (CZCS image, 25 November 1981) [17].

Similar Black Sea data dated 28 June 1979, shown in Fig. 9, illustrate the effect of massive river discharges in the coastal zone of an enclosed basin. The main feature of the whole Black Sea is in fact the high pigment concentration, possibly related to the combined effect of fluvial runoff, strong vertical stratification, and circulation features in general, on the presence and abundance of suspended and dissolved matter in surface waters. The extent of the impact of river discharges along the western coast (i.e., both a direct one owing to the sediment load and one induced on the planktonic flora by the nutrient load), from the Danube delta in particular, on the Black Sea surface colour field can be readily evaluated. The features traced by high pigments along the southern coast appear to be entrained in the interacting cyclonic circulations of the western and eastern sub-basins. Small plumes of high-pigment waters extending from the Bosphorus also seem to trace the Black Sea outflow into the Sea of Marmara (Fig. 9) [17].

The list of sensors that became available after CZCS for coastal/marine observations in the optical range, included the SeaSeaWIFS, in 1996; the ocean colour and temperature scanner (OCTS), also in 1996; the medium resolution imaging spectrometer (MERIS), and possibly follow-ups in the ERS family, in 1998; and the Earth observing system (EOS) suite of sensors, planned in the late 1990s as well, to name just a few [17].

The next tool that provided the ocean bio-geochemical remote sensing community with significant data was the SeaWiFS. The SeaWiFS Project Office was formally initiated by NASA in 1990. The sensor was finally launched by the Orbital Sciences Corporation in 1996 to provide five years of science-quality data for global ocean bio-geochemistry research. To date, the SeaWiFS program has greatly exceeded the mission goals established when it was launched in terms of data quality, data accessibility and usability, ocean community infrastructure development, cost efficiency, and community service. The SeaWiFS Project Office and its collaborators in the scientific community have made substantial contributions in the areas of satellite calibration, product validation, near-real-time data access, field data collection, protocol development, in situ instrumentation technology, operational data system development, and desktop level-0 to level-3 processing software [19].

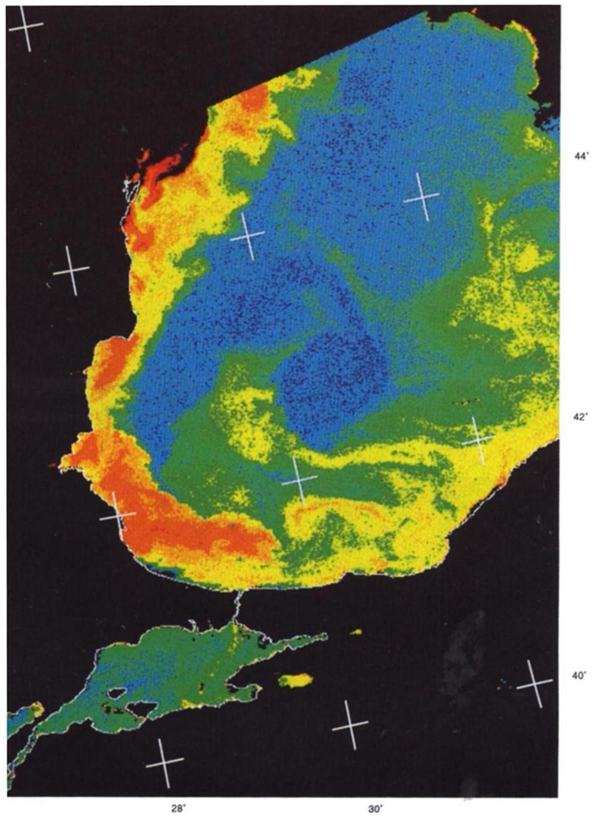

Fig. 9 Black Sea surface colour field (CZCS image, 28 June 1979) [17].

The riginal SeaWiFS program goals and project objectives were as follows:

- to determine the spatial and temporal distributions of phytoplankton blooms, along with the magnitude and variability of primary production by marine phytoplankton on a global scale,
- to quantify the ocean's role in the global carbon cycle and other bio-geochemical cycles,
- to identify and quantify the relationships between ocean physics and large-scale patterns of productivity,
- to understand the fate of fluvial nutrients and their possible effects on carbon budgets,
- to identify the large-scale distribution and timing of spring blooms in the global oceans,
- to acquire global data on marine optical properties, along with a better understanding of the processes associated with mixing along the edge of eddies and boundary currents, and
- to advance the scientific applications of ocean-colour data and the technical capabilities required for data processing, management, and analysis in preparation for future missions [19].

The quality of the data products of SeaWIFS was evaluated primarily on the comparisons with in situ data. For chlorophyll-a (chl-a), the slope and r^2 were 1.00 and 0.892 and 1.03 and 0.85, for 2804 match-ups and 262 match-ups, respectively, over a range of 0.03 to around 90 mg m^{-3} (Figs. 10a,b). The in situ data of Fig. 10a included only 113 cases from the Sargasso Sea and 35 cases from the North Adriatic (Mediterranean region) [19–21].

Standard SeaWIFS algorithms have been demonstrated to be inappropriate over the Mediterranean region. Therefore, in some papers uncertainties in the retrieval of satellite surface chl concentrations in the Mediterranean Sea have been evaluated using both regional and global (SeaWIFS)

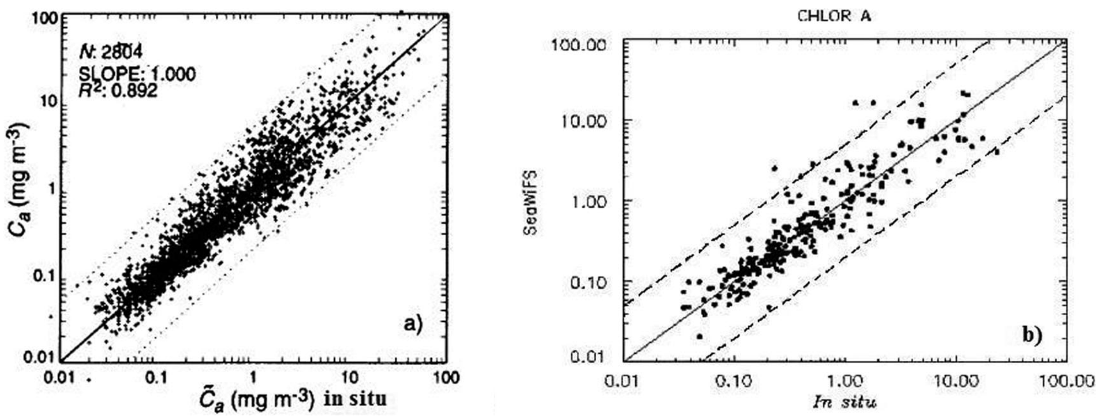

Fig. 10 Comparison of in situ and satellite chl a values: (a) algorithm OC4v4 data compared with in situ data 2804 match-ups [21], (b) algorithm OC4v4 data compared with in situ data 262 match-ups, fourth reprocessing of satellite data including all available improvements used by the SeaWifs Project Office [19].

ocean colour algorithms. The rationale for this effort was to define the most suitable ocean colour algorithm for the reprocessing of the entire SeaWiFS archive of the Mediterranean [22,23].

In one case, using a large dataset of coincident in situ chl and optical measurements, covering most of the trophic regimes of the Mediterranean basin, two existing regional algorithms and the global algorithm OC4v4 used for standard NASA SeaWiFS products were validated. The results of the analysis confirmed that the OC4v4 performs worse than the two existing regional algorithms, leading to a significant overestimation of the SeaWiFS-derived chl concentration (>70 % for chl <0.2 mg·m^{-3}). The two regional algorithms also showed uncertainties dependent on chl values. Then, a better tuned algorithm was introduced, the MedOC4. The results confirmed that MedOC4 is the best algorithm matching the requirement of unbiased satellite chl estimates and improving the percentage of the satellite uncertainty, and that the NASA standard chl products are affected by an uncertainty of the order of 100 %. Moreover, the analysis suggests that the poor quality of the SeaWiFS chl in the Mediterranean is not due to the atmospheric correction term but to peculiarities in the optical properties of the water column. Finally, the observed discrepancy between the global and the regional bio-optical algorithms has been discussed. The main result was the inherent bio-optical properties of the basin can explain the observed discrepancy. In particular, the oligotrophic water of the Mediterranean Sea is less blue (30 %) and greener (15 %) than the global ocean. Possible explanations for this are attributed to a proposed different phytoplankton community, structure and distributions in the Mediterranean, such as the presence of coccolitophores, the dominance of prokaryots, or a high ratio among eterotrophs and autotrophs [22].

In another research case (eastern Mediterranean, Cyprus eddy) the standard SeaWiFS OC4v4 algorithm generated data and MODIS chlor_a2 algorithm data overestimated chl-a as previously reported, while a regional algorithm proposed by Bricaud et al. 2002 [24] and the semi-analytical MODIS chlor_a3 algorithm gave improved retrievals (Fig. 11) [23].

SeaWiFS-derived (1998–2003) data were used to monitor algal blooming patterns and anomalies in the Mediterranean basin. Yearly and monthly means of chl-like pigment concentration were computed for these six years, and climatological means were derived (Fig. 12). The space and time patterns of the chl field appear to concur with the Mediterranean general oceanographic climate, while the chl anomalies describe trends and “hot spots” of algal blooming [18].

The analysis showed a general decrease of chl values in the yearly and monthly means and an earlier anticipation of the northwestern spring bloom, in comparison to what was seen in historical CZCS (1979–1985) data. These have been interpreted as symptoms of an increased nutrient limitation, resulting from reduced vertical mixing owing to a more stable stratification of the basin, in line with the gen-

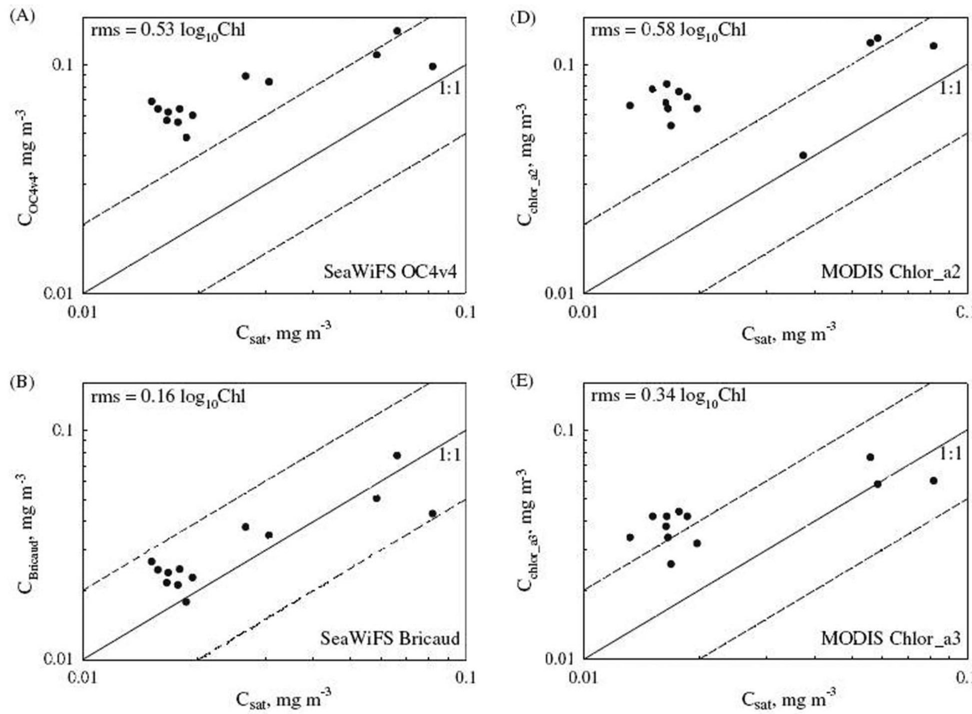

Fig. 11 SeaWiFS and MODIS retrievals compared to in situ data with different algorithms [23].

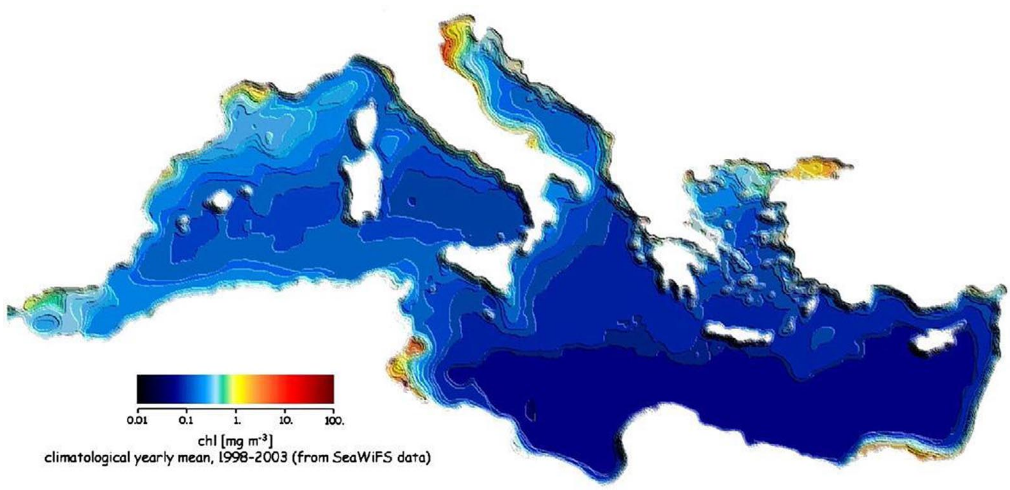

Fig. 12 SeaWiFS-derived (1998–2003) climatological chl yearly mean, Mediterranean Sea [18].

eral warming trend of the Mediterranean Sea in the last 25 years. At the same time, the recurrent increasing blooms at the various hot spots have been described as localized phenomena, linked to either air–sea interactions in pelagic domain (Lion and Rhodes gyres), or increased nutrient availability and low water renewal in coastal areas. The latter kind of anomalous blooms would be related to the anthropogenic impact on coastal sites (e.g., crowded beaches or marinas) or to the combination of specific geographical and meteorological conditions (e.g., enclosed bays during summer, when hydrodynamic forcing is low). This would suggest that noxious, or harmful, blooms (known to have occurred in the areas and periods considered) are predominantly local phenomena, with little or no connection to regional events [18].

In a study of the cycling of phosphorus in the Mediterranean, the (CYCLOPS) research team investigated phosphate limitation in the eastern Mediterranean at the centre of an anticyclonic eddy south of Cyprus. SeaWiFS mean chl-a maps were presented for the eastern Mediterranean for each month between September 1997 and August 2004. These maps (Fig. 13) showed that chl-a in the region decreased over the duration of the time series with reductions in the centre of the eddy, tracked using a quasi-Lagrangian approach, of approximately 33 % between 1997 and 1998 and 2002 and 2003. It was hypothesized that the variations in chl-a were partly a function of the eddy dynamics [23].

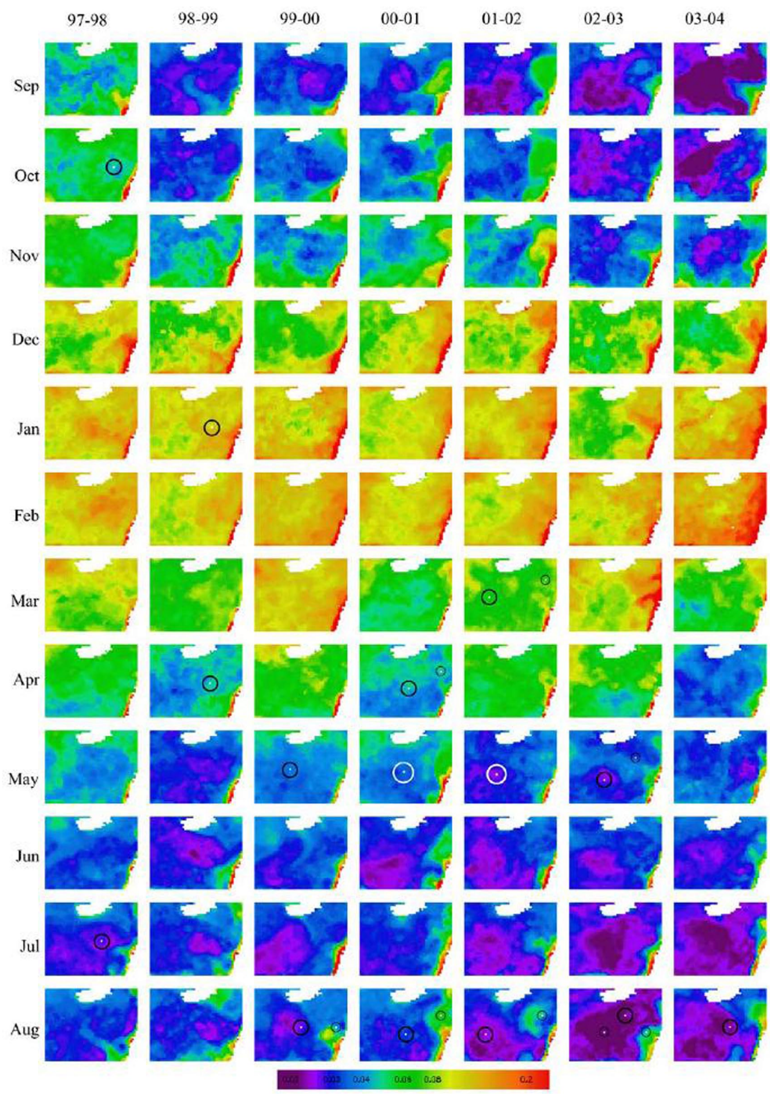

Fig. 13 Individual monthly chl-a maps using the B2002 algorithms with overlaid eddy centre locations determined from in situ observations: large black circle, “main” Cyprus eddy; small black circle, “secondary” eddies; large white circle, CYCLOPS cruises in May 2001 and 2002 [23].

In some cases, satellite remote sensing has been used to assess water quality in smaller scales, for example, particular coastal areas. Such an effort was the use of Landsat 7 ETM+ data in order to assess water quality in the coastal area of Tripoli (Lebanon) and provide a first baseline for coastal resources management. In situ data, collected in the field within 6 h before/after the time of the satellite overpass, were used to derive empirical algorithms for chl-a concentration, Secchi disk depth, and turbidity. Then, maps of the distribution of the selected water quality parameters were generated for the entire area of interest, and compared with analogous results obtained from SeaWiFS data. The maps indicate that the Tripoli coastal area is exposed to moderate eutrophic conditions along most of its shoreline (in particular, along the northern stretch), in correspondence with fluvial and wastewater runoff sources. The Landsat 7 ETM+ data proved useful for the intended application, and will be used to start a national database on water quality in the Lebanese coastal environment [25].

Another such effort to combine satellite and in situ monitoring was carried out by Greek researchers. The research was applied for the eastern coastal area of Lesvos Island. The concentration of chl-a, water transparency, and SST were measured in situ at the date and time of satellite overpass (Fig. 14). The aim of the study was to assess the ability to determine the above-mentioned parameters by Landsat-TM satellite images [26].

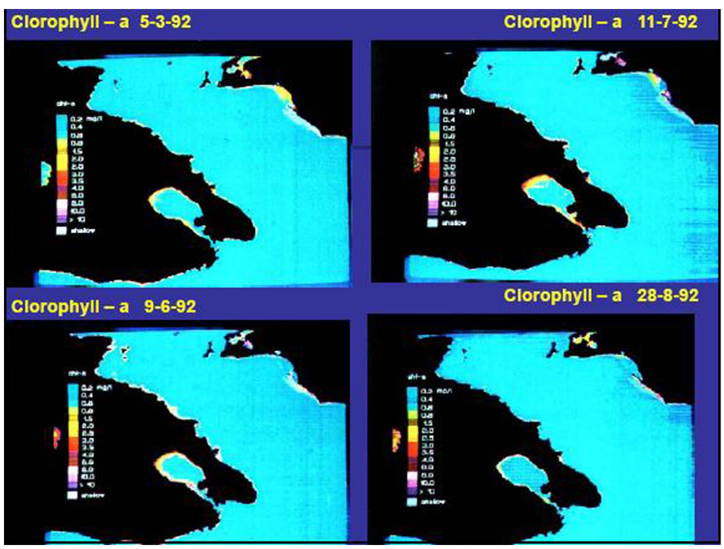

Fig. 14 Landsat-TM satellite images of chl-a in Lesbos straits (Greece) [26].

Finally, in the case of local water quality monitoring of coastal areas a similar approach has been to use aircraft-carried sensors. In such a research activity, the hyperspectral compact airborne spectrographic imager (CASI) sensor was implemented to monitor water quality in a transitional zone from polluted to clean sea-water, in Haifa Bay and adjacent river estuaries, at the northern part of the Mediterranean coast of Israel. Synoptic measurements of optical data acquired from the airborne scanner were used to map chl-a and suspended particulate matter (SPM) concentrations in surface waters in the study area (Fig. 15). This airborne hyperspectral scanner was found to be an expedient monitoring tool for the relatively small geographic area of the current study, as it was able to reveal the patchy distribution and sharp concentration changes of the mapped water characteristics. The chl-a concentrations mapped and measured in this survey were unusually low (<2 $\mu g \cdot dm^{-3}$) owing to a long-period intermission of anthropogenic phosphate and nitrate input to the bay. The SPM and chl-a spatial distribution

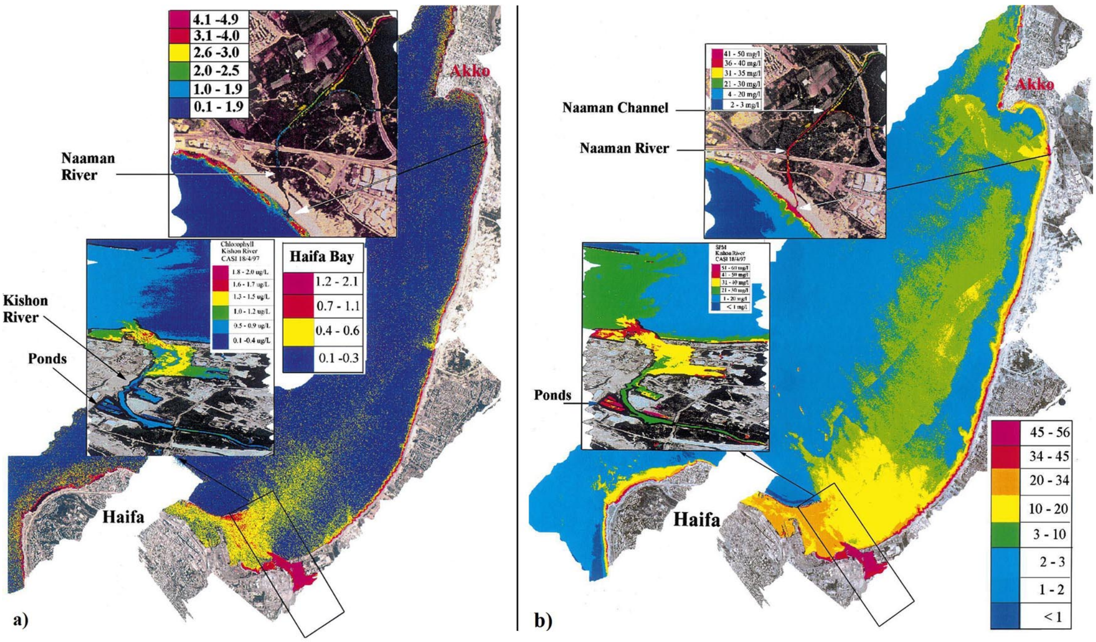

Fig. 15 Spatial distribution of (a) chl-a ($\mu g \cdot dm^{-3}$) and (b) SPM ($mg \cdot dm^{-3}$) concentrations (Haifa Bay) [27].

along the lower river system exhibit variations which could be plausibly explained by the hydrological structure and geochemical impacts on the riverine water sources [27].

One of the latest and most advanced applications of remote sensing ocean colour is the distribution of phytoplankton to size types or classes from satellite data. Until recently, the principal goal of satellite-borne sensing of ocean colour was to create synoptic fields of phytoplankton biomass (as chl-a concentration). In the context of climate change, a major application has been the modeling of primary production and the ocean carbon cycle. It is now recognised that a partition of the marine autotrophic pool into a suite of phytoplankton functional types (PFTs), each type having a characteristic role in the bio-geochemical cycle of the ocean, would increase our understanding of the role of phytoplankton in the global carbon cycle. At the same time, new methods have been emerging that use visible spectral radiometry to map some of the PFTs. Attempts to identify PFTs from space represent a new development, with potential for further improvement, owing to the increasing improvement in both spectral and radiometric resolution of satellite sensors as well as the understanding of phytoplankton optical properties. But it is just as important to realise that remote sensing cannot provide all the answers. What is needed is a judicious combination of in situ and remote sensing techniques, to help extract maximum information on the distribution of PFTs at the global scale [28].

A model has been developed that is able to link phytoplankton absorption to phytoplankton size classes (PSCs). This model uses the optical absorption by phytoplankton at 443 nm, symbolized aph(443), which can be derived from the inversion of ocean colour data. The model is based on the observation that the absolute value of aph(443) co-varies with the spectral slope of phytoplankton absorption in the range of 443–510 nm, which is also a characteristic of PSCs. The model, used for SeaWiFS global data, showed that picoplankton (0.2–2 μm) dominated in surface waters (~79.1 %), nanoplankton (2–20 μm) followed (~18.5 %), and microplankton (20–200 μm) constituted the remainder (2.3 %). The Atlantic and Pacific oceans showed seasonal cycles with both micro- and nanoplankton increasing in spring and summer in each hemisphere, while picoplankton, dominant in the oligotrophic gyres, decreased in the summer. The PSCs derived from SeaWiFS data were verified by comparing contemporary 8-day composites with PSCs derived from in situ pigment data from quasi-concurrent Atlantic Meridional Transect cruises [29].

8. REMOTE SENSING MONITORING OF SPM COASTAL ZONE GEOLOGICAL FEATURES

Applications of remote sensing to geological features of coastal zones have also been reported. In the coastal area of Haifa (Israel), synoptic measurements of optical data acquired from an aircraft-carried scanner were used to map SPM concentrations in surface waters in the study area (Fig. 15b). The distribution of SPM concentrations in Haifa Bay was mainly dictated by the polluted riverine inputs, with concentrations between 1 and 3 mg/L at its seaward border and higher by more than one order of magnitude at the river estuary. The correlation between SPM and some particulate heavy metal concentrations was found as a useful tool for monitoring such environmental hazardous substances [27].

In the case of coastal zones, it is widely acknowledged that Natura 2000 areas should be monitored to ensure the maintenance or restoration of their composition, structure, and extent. The ESA's GlobWetland project provided remotely sensed products for several Ramsar wetlands worldwide, such as detailed land cover/land use, water cycles, and inundated vegetation maps. In the case of Greece, a research team presented an operational methodology for updating a wetland's habitat map using the GlobWetland products [30].

The existing habitat maps of five Greek Ramsar wetlands (artificial lake Kerkini, Amvrakikos gulf, Kotychi lagoons, lakes Koronia-Volvi, and the delta of Axios-Loudias-Aliakmonas rivers), which had been developed for the Ministry of Environment and the European Union in 2001 were updated using these methodologies. The developed methodology was proven successful in its application to these resulting habitat maps met the European and Greek national requirements (Fig. 16, Table 1). Results revealed that GlobWetland products were a valuable contribution, but source data (enhanced satellite images) were necessary to discriminate spectrally similar habitats. Finally, the developed methodology can be modified for original habitat mapping [30].

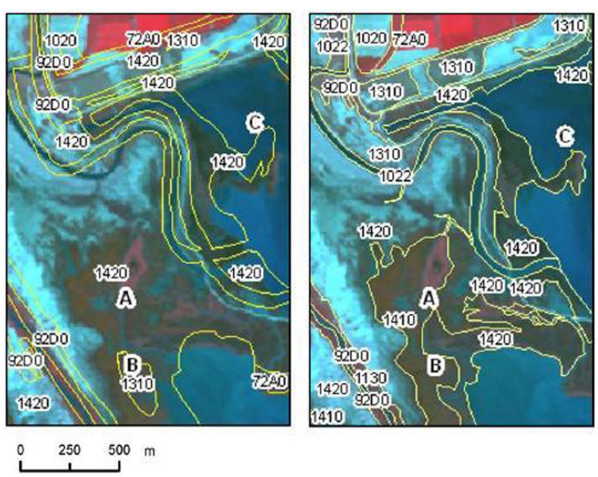

Fig. 16 The habitat map of 2001 using the original methodology and the updated habitat map using the proposed remote sensing methodology (Axios delta). Habitat codes listed in Table 1 (adapted from ref. [30]).

Table 1 Habitat codes.

Habitat code	Habitat description
1061[a]	Unvegetated sandy substrates
1130	Estuaries
1150[b]	Lagoons
119B[a]	Vegetated soft substrates
1310	*Salicornia* and other annuals colonising mud and sand
1410	Mediterranean salt meadows (*Juncetalia maritimi*)
1420	Mediterranean and thermo-Atlantic halophilous scrubs (*Arthrocnemetalia fructicosae*)
3150	Natural eutrophic lakes with *Magnopotamian* or *Hydrocharition*-type vegetation
3280	Constantly flowing Mediterranean rivers: *Paspalo-Agrostidion* and hanging curtains of *Salix* and *Populus alba*
32B0[a]	Muddy banks of Euro-Siberian rivers with annual vegetation
6290[a]	Mediterranean subnitrophilus grasslands
651A[a]	Mesophile pastures
72A0[a]	Reed beds
92A0	*Salix alba* and *Populus alba* galleries
92D0	Thermo-Mediterranean riparian galleries (*Nerio-Tamariceteae*) and southwest Iberian Peninsula riparian gallers (*Securinegion tinctoriae*)

[a]Habitats not included in Annex I of the habitats directive.
[b]Priority habitat type according to Annex I.

In another instance, a combination of remote sensing, field surveys, and sedimentological analysis of beach sands was used to assess changes of the shorelines of the Nile delta in general and specifically at Damietta owing to the construction of a harbour. Very dynamic coastlines, such as sections of the Nile delta coast, pose considerable hazards for human structural use and development, and rapid, replicable techniques are required to update coastline maps of these areas and monitor rates of movement. The synoptic capability of Landsat-TM imagery enables monitoring of large sections of coastline at relatively coarse 30 m spatial resolution. By comparing positions of the Nile delta coast in 1984, 1987, and 1990–1991, mapped using a region-growing image segmentation technique, areas of rapid change can be identified and targeted for more detailed monitoring in the field, or using higher-resolution images. Rates of erosion and deposition can be estimated crudely, and areas where change appears to be accelerating can also be identified. Areas of severe erosion along the Nile delta coast are found to be confined to the promontories of the present-day mouths of the Nile River at Rosetta and Damietta. The results indicated that harbour construction, and, in particular, the construction of two jetties that extend out from the harbour entrance, have created a discontinuity in the eastward-moving littoral drift. Significant shoreline advance extends a considerable distance west of the western jetty (Fig. 17a), and significant shoreline recession extends a considerable distance east of the eastern jetty (Fig. 17b). Conventional bathymetric surveys highlight changes in the near-shore environment associated with the growth of the up-drift accretionary wedge and siltation of the harbour access channel. The synergistic use of remote sensing, bathymetric surveying, and sedimentology provides evidence that changes have affected a much larger area than predicted at the time of harbour construction [31,32].

Remote sensing has also been deemed as promising in identifying fracture zones on the Earth's surface especially when field surveys fail to trace and identify them in arid regions, characterized by flat topography and where sand dunes extensively cover the terrain. It is deemed possible to identify the regional fractures as lineaments on remotely sensed images or shaded digital terrain models. In such research, a segment tracing algorithm (STA), for lineament detection from Landsat-7 Enhanced Thematic Mapper Plus (ETM+) imagery, and the data from the Shuttle Radar Topographic Mission (SRTM) 30 m DEM, were applied in the Siwa region (northwest of the Western Desert of Egypt). The objectives were to analyze the spatial variation in orientation of the detected linear features and its rela-

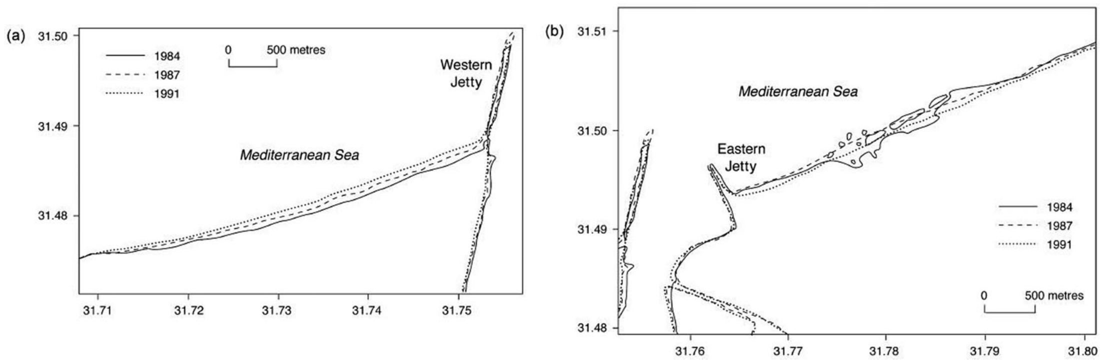

Fig. 17 Maps showing the changes in shoreline position to the (a) west and (b) east of Damietta Harbour, produced by automatic segmentation of Landsat-TM imagery. Shoreline positions are mapped at 1984, 1998, and 1991 (adapted from ref. [32]).

tion to the hydrogeologic setting in the area and the underlying geology, and to evaluate the performance of the algorithm applied to the ETM+ and the DEM data. Detailed structural analysis and better understanding of the tectonic evolution of the area could provide useful tools for hydrologists for reliable groundwater management and development planning [33].

Remote sensing has also been used to reveal buried river channels in a number of regions worldwide, in many cases providing evidence of dramatic paleoenvironmental changes over Cenozoic time scales. Using orbital radar satellite imagery, a major paleodrainage system in eastern Libya was mapped. This paleodrainage system could have linked the Kufrah basin to the Mediterranean coast, possibly as far back as the middle Miocene. SAR images from the PALSAR sensor revealed a 900-km-long river system, which started with three main tributaries that connected in the Kufrah oasis region. The river system then flowed north and formed a large alluvial fan. The sand dunes of the Calanscio Sand Sea prevented deep orbital radar penetration and precluded detailed reconstruction of any possible connection to the Mediterranean Sea, but a 300-km-long link to the Gulf of Sirt through the Wadi Sahabi paleochannel is likely. If this connection is confirmed, and its Miocene antiquity is established, then the Kufrah River, comparable in length to the Egyptian Nile, will have important implications for the understanding of the past environments and climates of northern Africa from the middle Miocene to the Holocene [34].

Remote sensing techniques have also been combined with field investigations in order to locate and accurately characterize volcanic structures. The detection of caldera structures, apart from its usefulness in volcanological studies, is also of great interest for applied ore deposit research for epithermal precious metal mineralization in geothermal fields. Such an application was reported for the volcanic field of Lesvos Island, in which volcanic structures were difficult to recognize owing to erosion and faulting. Landsat-TM and Satellite Pour Observer la Terre Panchromatic (SPOT-Pan) satellite images as well as the DEM of the study areas were digitally processed in order to reveal specific geological characteristics related to caldera structures such as topographic caldera rims and floors, ring faults, areas of hydrothermal alteration, drainage networks, and lava domes, both internal and external to caldera structures. Six caldera structures were recognized, of which four have been identified for the first time. A combination of remote sensing and fieldwork data was used for the detection and mapping of the Miocene calderas. The relevant output images were generated from the analysis and processing of: (1) a Landsat-TM satellite image of Lesvos Island, with a spatial resolution of 30 × 30 m pixel size, acquired on 20 August 1999; (2) a SPOT-Pan satellite image of the same area, with a spatial resolution of 10 × 10 m pixel size, acquired on 12 July 1999; and (3) the DEM with a cell size of 30 m, which was obtained by digitizing the elevation contour lines of the 1:50000 scaled topographic maps of the study area. It is a continuous raster layer of the island, in which data values represent elevation, generated from the 30 m contours of the topographic maps. The satellite data were pre-processed in order to remove the geometric distortions and to bring the remote sensing images into registration with one another. With the use of topographic maps of the study area, the images were geometrically corrected and geo-referenced based on the Hellenic Geodetic Reference System (HGRS ’87) [35].

9. REMOTE SENSING MONITORING OF BIOTA

The tools of remote sensing have also been used, but to a lesser extent, for biological oceanography applications. One of the research fields is the mapping of sea grasses, such as the protected species *Posidonia Oceanica*, which is the dominant sea grass in the Mediterranean Sea and is known to affect bio-geochemical and physical processes in coastal areas. The widespread loss of this species is attributed to excessive anthropic pressure and other large-scale environmental changes. Sea grass conservation requires mapping to estimate the extent of existing stocks and to measure changes over time. Optical remote sensing provides a cost-effective method to monitor vast areas of shallow waters that are potential *P. oceanica* habitats. As part of an interdisciplinary research effort, where the effects of these sea grasses on the hydrodynamics were investigated, new technologies of reliable, fast, and effective monitoring of *P. oceanica* were essential. A published method used IKONOS multispectral imagery for bottom classification in a shallow coastal area of Mallorca (Balearic Islands). After applying a supervised classification, pixels were automatically classified in four classes: sand, rock, *P. oceanica* bottoms, and unclassifiable pixels (Fig. 18). Results indicated that, in these clear waters, the spectral response of *P. oceanica* can be determined to a depth of about 15 m. In order to validate the method, the image classification was compared with a bottom classification derived from an acoustical survey. Agreement with the reference acoustic seabed classification was up to 84 % for the sampled area. Thus, spectral IKONOS image analysis was presented as an effective approach for monitoring *P. oceanica* meadows in most clear, shallow waters of the western Mediterranean [36].

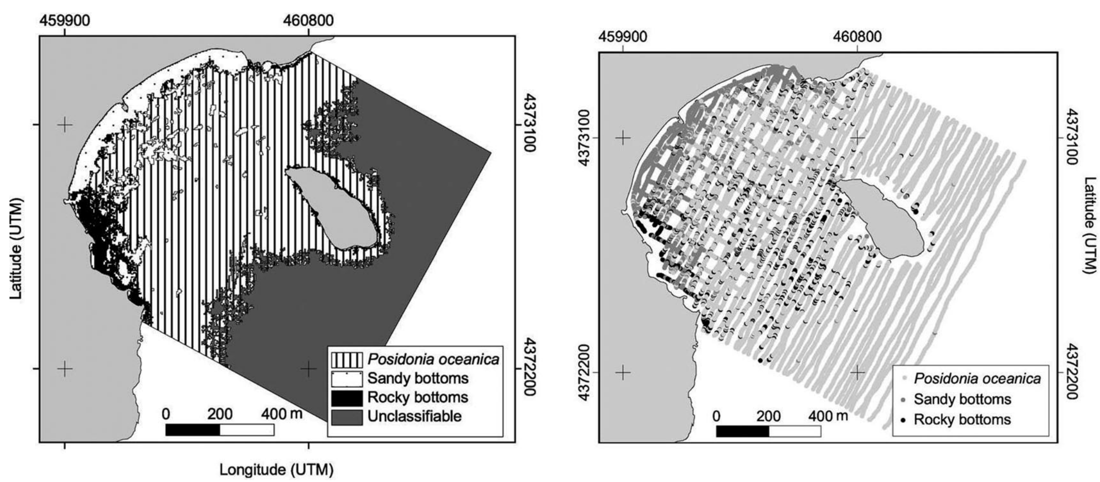

Fig. 18 Bottom types derived from the IKONOS satellite images (left) and acoustical survey (right) [36].

In another study, multispectral imagery with a spatial resolution of 10 m and fused imagery with a spatial resolution of 2.5 m from the SPOT 5 satellite were used for mapping beds of *P. oceanica* in the Mediterranean Sea (Laganas Bay, Zakynthos, Greece, *Caretta carreta* habitat), where it is a dominant species. *Posidonia* forms monospecific beds in a structurally simple environment, where four classes can be identified: sand, photophilous algae on rock, patchy sea grass beds, and continuous sea

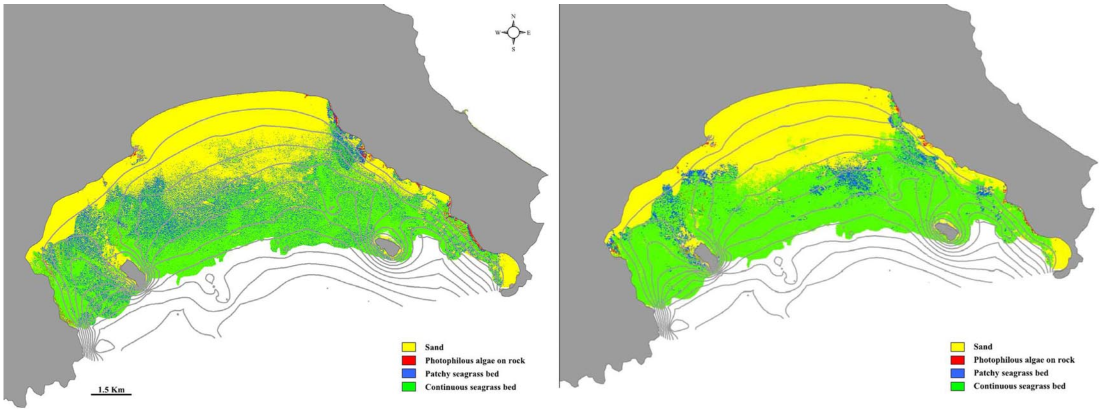

Fig. 19 Maps of the benthic assemblages and bottom types (Laganas Bay, pixel size 2.5 m, left, and 10 m, right) [38].

grass beds (Fig. 19). A direct comparison of overall accuracy between SPOT 2.5 m and SPOT 10 m revealed that this tool provided accurate mapping in both cases (between 73 and 96 % accuracy). Although SPOT 2.5 m provided lower overall accuracy than SPOT 10 m, it is a very useful tool for the mapping of *P. oceanica*, as it allows the patchiness of the formations to be better taken into account [37].

A Greek research team has shown that the introduction of warm and tropical alien species in the Aegean and Ionian seas has been exacerbated by the observed warming of the eastern Mediterranean Sea. The phenomenon has accelerated after an abrupt shift in both regional and global temperatures that we detect around 1998, leading to a 150 % increase in the annual mean rate of species entry after this date. Abrupt rising temperature since the end of the 1990s has modified the potential thermal habitat available for warm-water species, facilitating their settlement at an unexpectedly rapid rate. For the statistical correlations, the following types of data were used: (A) long-term data of 149 warm alien species from 1924–2007 obtained from the list available at the Ellenic Network on Aquatic Invasive Species (ELNAIS) web site, which is archived in the Hellenic Centre for Marine Research and updated with every new record and regularly reported; (B) SST data (AVHRR, NOAA, 1985–2007); (C) northern hemisphere temperature (NHT) anomalies, obtained from the Climatic Research Unit and Hadley Centre from 1850 to 2007; and (D) regional air temperature data that were collected and provided from the meteorological stations of the Hellenic National Meteorological Service (HNMS) at 15 stations (north, middle, and south Aegean and eastern Ionian seas). The speed of alien species spreading and response to global warming is apparently much faster than temperature increase itself, presenting an important warning for the future of Mediterranean Sea biodiversity [38].

Some studies have tried to explain distributions and habitat preferences of cetaceans. In one such study, habitat use and preferences of fin whales and striped dolphins were modeled in order to provide information on critical habitats for cetaceans and meet the needs of the Pelagos Sanctuary for the Conservation of Mediterranean Marine Mammals (between southeastern France, Monaco, northwestern Italy, and northern Sardinia, and encompassing Corsica and the Tuscan Archipelago). In order to produce the desired information sighting, data collected between 1993 and 1999, explanatory physiographic variables (mean, range, and standard deviation of depth and slope, and distance from the nearest coastline), and remotely sensed data (SST and chl-a concentration from AVHRR and SeaWiFS sensors) were considered in the models. Generalized additive models (GAMs) were used to model the distribution of fin whales and striped dolphins in relation to these variables, and “classification and regression trees” were used for habitat characterization and predictive models. SST values were indicators of striped dolphin and fin whale presence, with both species showing a tendency to prefer colder waters (21–24 °C). The classification also indicated an importance of chl-a for both species. The techniques applied to this dataset proved to be valuable tools to describe habitat use and preferences of cetaceans, and the use of the remotely sensed data can substantially improve the predictions [39].

In another case, the summer distribution pattern of fin whales (*Balaenoptera physalus*) in the northwestern Mediterranean Sea was evaluated. Satellite imagery was used to gain knowledge on primary biomass over large time and space scales. Net primary production (NPP in $g{\cdot}C{\cdot}m^{-2}{\cdot}day^{-1}$), was estimated by processing remote-sensed measurements of chl concentration, provided by SeaWIFS, and additional variables were derived from SST (AVHRR/NOAA sensors). Fin whale distribution was obtained from survey data and expressed in sightings per unit of effort. Multiple cross-correlation coefficients were calculated between these environmental parameters and the fin whale summer distribution from 1998 to 2002. A predictive model was developed from this statistical approach, and the understanding of the variability of fin whale distribution in summer was improved. While food availability at a particular time and place is a function of environmental conditions in the previous months, this study provides evidence that whales adapt their movements and group size directly to food availability rather than to instantaneous environmental conditions [40].

10. REMOTE SENSING MONITORING OF OIL SPILLS: SENSORS AND CASE STUDIES

Apart from natural marine processes (temperature and phytoplankton distributions), oil pollution is an area of great public concern in regional seas. The majority of marine oil spills result from ships emptying their billage tanks before or after entering port. Large-area oil spills result from tanker ruptures or collisions with reefs, rocky shoals, or other ships as well as oil platform accidents. These spills are usually spectacular in the extent of their environmental damage and generate widespread media coverage. Routine surveillance of shipping routes and coastal areas is necessary to enforce maritime pollution laws and identify offenders [41,42].

Remote sensing offers the advantage of being able to observe events in remote and often inaccessible areas. For example, oil spills from ruptured pipelines may go unchecked for a period of time because of uncertainty of the exact location and extent of the spill. Remote sensing can be used to both detect and monitor spills. For ocean spills, remote sensing data can provide information on the rate and direction of oil movement through multitemporal imaging and input to drift prediction modeling, and may facilitate in targeting clean-up and control efforts [41].

Remote sensing devices used include IR video and photography from airborne platforms, TIR imaging, airborne laser fluorosensors, air- and spaceborne optical sensors, as well as air- and spaceborne SAR [41]. Because of the importance of oil spill detection, firstly, air- and spaceborne sensors will be adequately reviewed and evaluated in terms of their usefulness, and, secondly, some case studies of oil spill remote sensing will be presented [43].

The oldest and less expensive applications were based on optical sensors mounted in aircraft. In the *visible region* of the electromagnetic spectrum (approximately 400–700 nm), the oil slicks appear silver–grey to brown and there is also a change in the texture of the sea surface. The sunlight interferes and obscures the presence of the oil. Furthermore, there are many other interferences or false alarms (sun glint, wind sheens, surface seaweeds, or sunken kelp beds). The use of visible techniques (photographs, video) in oil spill remote sensing is largely restricted to documentation, but it is still an economical way, since there is no need for dedicated aircraft [41,43].

Oil absorbs solar radiation and re-emits a portion of it as thermal energy, in the 8–14 μm region. The detection of oil in the *IR region* is based on the temperature difference between the oil and the water or on the difference in emissivity. In IR images, thick oil appears hot, intermediate thicknesses of oil appear cool, and thin oil or sheens are not detected. The thicknesses at which these transitions occur are poorly understood, but evidence indicates that the minimum detectable layer is between 10 and 70 μm. Unfortunately, near-IR detection is characterized by low sensitivity (detected temperature differences over 2 °C), while there are available mid-IR cameras that can detect temperature differences as small as

0.02 °C. In TIR, slicks of thicknesses between 50 and 500 μm appear to be at a lower temperature than the surrounding water. The oil is a less effective emitter than the water and hence appears cooler. In this case, the detection of the oil does not depend on solar radiation, so a TIR detector can operate both day and night. Acceptable TIR systems for detecting oil on water must detect temperature differences of less than 0.2 °C. The advantages of near-IR, mid-IR, and TIR systems are that they are relatively simple to operate, the output is easy to interpret, they are lightweight, they consume little power, they are suitable for mounting in aircraft of opportunity, and, finally, they are moderately expensive. Furthermore, TIR systems can operate both day and night, they can easily differentiate between oil and other natural objects, and they can distinguish between sheen and thick oil and detect thickness gradients. A major disadvantage of any type of IR detector, however, is that they require cooling to avoid thermal noise, which would overwhelm any useful signal. Liquid nitrogen, lasting about 4 h, has traditionally been used but new, smaller sensors use closed-cycle or Joule–Thompson coolers, which operate on the cooling effect created by expanding gas; even though a gas cylinder or compressor must be transported with this type of cooler, refills or servicing may not be required for days at a time. Other disadvantages of IR sensors are that they cannot penetrate cloud, they cannot operate at night (near- and mid-IR), they produce many false targets from plant material (near-IR), and small-scale temperature changes, which occur owing to the complex circulation patterns in the ocean and produce patterns that might be confused with oil (mid-IR). They cannot be used through a regular window of an aircraft, and the detector must be either mounted without a window or by using a germanium window (mid-IR and TIR) and finally they measure absolute oil thickness, and the application of dispersant causes significant changes in the emissive properties of the oil and can confuse the interpretation of the images (TIR). Most IR systems produce a standard television output, which can be displayed and recorded. Using this method of output, it is easy to obtain and record an image in a compact format. If further analysis of the image is required, the television format is converted into a computer-readable format with a frame grabber. IR cameras are very common, and commercial units are available from several manufacturers [41,43].

In the *UV*, the reflectivity of oil and water are different. The reflectivity of oil in the UV is 1.02, whereas that of water is 0.722. Since reflectivity is a surface phenomenon, any hydrocarbon on the surface, independent of thickness, will be detected. Therefore, UV sensors can be used to map sheens of oil as oil slicks display high reflectivity of UV radiation even at thin layers (<0.01 μm). Most UV systems use a standard television camera with a suitable filter package. The advantages of UV systems are that they are simple, lightweight, and require little power, they are suitable for mounting in aircraft of opportunity, they produce a video output easy to display and record, and they are relatively inexpensive. The disadvantages of UV systems are that they detect the presence of any hydrocarbon on the water surface and cannot differentiate between sheen and thicker oil slicks, and they can only operate under daylight conditions with clear visibility. They are also subject to many interferences or false images such as wind slicks, sun glints, and biogenic material. Overlaid UV and IR images are often used to produce a relative thickness map of oil spills and since the UV interferences are often different than those for IR sensing, combining IR and UV can provide a more positive indication of oil than using either technique alone [41,43].

When the oil is excited, using intense UV radiation from a laser, a fluorescence return, which is unique to the presence of oil on the water surface, can be detected. The *laser fluorosensor* is a complex instrument that can identify and classify the presence of oil on water and shorelines. Natural fluorescing substances, such as chl and *gelbstoff* or yellow matter, fluoresce at sufficiently different wavelengths than oil. As different types of oil yield slightly different fluorescent intensities and spectral signatures, it is possible to differentiate between classes of oil under ideal conditions. The fluorescent response of crude oil ranges from 400 to 650 nm with peak centres in the 480 nm region. Laser fluorosensors have significant potential as they may be the only means to discriminate between oiled and un-oiled seaweeds and to detect oil on different types of beaches. Tests on shorelines have been very successful, and algorithms have been developed. The fluorosensor is also the only reliable means of detecting oil in certain ice and snow situations. The advantages of laser fluoresensors are that they are active systems and hence can operate both by day and night, they can positively differentiate oil from other surface materials, and they can provide an indication of the type of oil on the water. The disadvantages of laser fluorosensors are that they are generally bulky and require a significant amount of power, they are presently point detectors, and they operate in the UV and visible bands and hence cannot operate under conditions of fog or cloud [41,43].

The ocean emits *microwave radiation*. Oil on the ocean emits stronger microwave radiation than the water and thus appears as a bright object on a darker sea. This detection method has not been very successful in the field, however, as several environmental and oil-specific parameters must be known. Microwave radiometers are passive sensors that measure the naturally emitted and reflected radiation from the ocean surface, and if the wavelength is chosen to be longer than the oil thickness, then it is possible to measure the relative thickness of the oil film. The advantages of microwave radiometers are that they have all-weather operational capability, except in heavy rain, and they are an imaging system with the potential to measure relative thickness. The disadvantages of microwave radiometers are that they require a special antenna and hence a dedicated aircraft, they are expensive and complex to operate, there is limited experience with microwave radiometers in field situations, and the limited spatial resolution causes averaging over a large area of the slick. Oil slick non-homogeneities are smaller than the sensor footprint, which results in the determination of the average value of the oil thickness integrated over a large area [41,43].

Capillary waves on the ocean reflect radar energy, producing a "bright" image known as sea clutter. Since oil on the sea surface dampens some of these capillary waves, the presence of an oil slick can be detected as a "dark" sea, with an absence of this sea clutter. The two basic types of radar that can be used for environmental remote sensing in general and specifically for oil spills are SAR and SLAR. The latter is an older, but less expensive technology, which uses a long antenna to achieve spatial resolution. SAR uses the forward motion of the aircraft to synthesize a very long antenna, thereby achieving very good spatial resolution, which is independent of range, at the expense of sophisticated electronic processing. While inherently more expensive, the SAR has greater range and resolution than the SLAR. In fact, comparative tests show that SAR is vastly superior. There are many interferences or false targets, including fresh water slicks, wind slicks (calms), wave shadows behind land or structures, seaweed beds that calm the water just above them, biogenic oils, and whale and fish sperm. Radar is also limited by sea state. Sea states that are too low will not produce enough sea clutter in the surrounding sea to contrast to the oil, and very high seas will scatter radar sufficiently to block detection inside the troughs. Indications are that minimum wind speeds of 1.5 m/s (~3 knots) are required to allow detectability and a maximum wind speed of 6 m/s (~12 knots) will again remove the effect. Despite these limitations, radar is an important tool for oil spill remote sensing because it is the only sensor that can be used for searches of large areas and it is one of the few sensors that can "see" at night and through clouds or fog. In summary, SAR is still the most efficient and superior satellite sensor for oil spill detection and can be proven useful in oil spill remote sensing, particularly for searches of large areas and for night-time or foul weather work despite the fact that the technique is highly prone to false targets and limited to a narrow range of wind speeds [43,44].

As in the case of other sensors and applications (SST, chl a), it has been considered important to calibrate remotely sensed oil data. In one research paper, by De Domenico et al. 1994 [45], oil pollution levels were estimated using simultaneous acquisition of data from remote sensing by helicopter and fluorescence spectroscopy on surface samples. Laboratory quantitative analysis of hydrocarbons was used to calibrate remotely sensed data. The data acquired by the mentioned techniques were treated using a computer to generate a colour-coded map not attainable with conventional methods representing seawater pollution. Results, obtained in an oil-polluted bay (Augusta Bay, Sicily) with the two different methodologies, were in good agreement and indicated that remotely sensed data together with those achieved by fluorescence spectroscopy are applicable for monitoring hydrocarbon pollution. Comparison between the remote sensing output and the isopleths obtained through UVF fluorescence analysis showed a quite good concordance of hydrocarbon distribution [45].

The signal processing is very detrimental to oil spill detection. There are manual approaches and automatic algorithms for oil spill detection. Detection of oil spills can be divided into the following steps: (a) detection of suspected slicks, (b) manual verification of the slicks (oil/look-alike), and (c) assignment of confidence levels. An example of manual oil slick detection from SAR images is the case of KSAT (Kongsberg Satellite Services AS) in Norway that has provided a manual oil spill detection service since 1994. Here, operators are trained to analyze SAR images for the detection of oil pollution. The KSAT approach has been described by Indregard et al. 2004 [46]. External information about wind speed and direction, location of oil rigs and pipelines, and national territory borders and coastlines are used as support during the analysis. The operator uses an image viewer that can calculate some spot attributes, but he/she still has to go through the whole image manually. This is time-consuming. Possible oil spills found are assigned high, medium, or low confidence levels. The assignment is based on the following features: the contrast level to the surroundings, homogeneity of the surroundings, wind speed, nearby oil rigs and ships, natural slicks nearby, and edge and shape characteristics of the spot. The determination of a confidence level is not exact science, and there will always be an uncertainty connected to the results from manual inspection. During manual inspection, contextual information is an important factor in classifying oil spills and look-alikes. A challenge is to somehow incorporate the expert knowledge into automatic algorithms [44].

A study of best practices has been performed by the Oceanides project [46], implementing a comparison between the KSAT manual approach, the NR automatic algorithm (described by Bjerde et al., 1993; Solberg and Solberg, 1996; Solberg and Volden, 1997, Solberg et al., 1999, 2003 [47–51]) and QinetiQ's semi-automatic oil spill detection approach. QinetiQ's semi-automatic approach covers only the first step of an automatic algorithm, dark spot detection, and therefore the output targets must be classified visually by an operator. In this study, the three satellite-based approaches were compared to airborne verifications in a satellite-airborne campaign. The study was done without the operators or the algorithms knowing of the aircraft verifications. (The benchmark set consisted of 32 RADARSAT-1 images.) This dataset contained 17 verified oil spills. KSAT detected 15 of these slicks, NR's algorithm detected 14, and QinetiQ detected 12. The results show that a challenge is to have all operators pick out the same spots and assign the same confidence levels. NR's algorithm is objective and produces the same result repeatedly. Good agreement was found for high-contrast slicks among the various methods, but there were some differences on low-contrast slicks. The operators at KSAT use 3–25 min to analyze a scene (on average, 9 min), the NR's algorithm used about 3 min, and QinetiQ's algorithm used 20 min per scene on average. This shows that automatic approaches are more feasible as the volume of SAR data increases [44].

In the case of satellite imagery for oil spills, there are many problems of data transmission and analysis that cause significant time delays in the production of the imagery. Images more than 2–3 h old have only limited value for tactical purposes owing to the dynamic nature of an oil slick. These time delays, combined with the infrequent passes of many satellites, cause some doubts about the usefulness of satellites for the remote sensing of oil on water, however, they can definitely be utilized in determining ocean and wind fields for trajectory models [41].

The wrecking of tankers may occur close to a coast or far from it. In the first case, weather conditions permitting, an assessment of the oil spill extent and potential damage, as well as post-disaster oil spill tracking and monitoring. It can be performed by airborne missions provided that the coasts belong to countries that possess adequate airborne surveillance infrastructures. In the second case, operational considerations may prevent the use of airborne systems, and, therefore, satellites appear to be the only alternative for an early assessment of the disaster's extent and the subsequent monitoring of oil spills. In the case of a disaster, the position of a distressed tanker is a priori known by a radioed S.O.S. message; and this information can be used to command the satellite, so that its sensors will be directed to look at the disaster area with minimum delay. The detection of an oil spill, resulting from a tanker's wreckage, is required within the first 12–24 h from the time the accident has occurred. In addition, subsequent revisits of the disaster area are required at intervals of 24 h or less, to monitor oil slick migration due to local currents. Owing to the necessary high revisit frequency to the disaster area, a single satellite system will not be adequate to satisfy all mission performance requirements, especially considering reliability and availability. Accordingly, a satellite observation system should be based on a constellation of satellites, their number depending on the required revisit interval and field-of-view of the sensors. Since the mission will also require all weather and day/night capabilities, to meet the high revisit frequency operational profile, each satellite should be equipped, if not exclusively, with a radar sensor. SARs are ideal for this task because they provide a cross-track ground resolution independent of the slant range. Resolution-wise, oil spill detection and tracking requires about 30–50 m ground resolution capability, although a better resolution around 10–15 m would be more suitable to evaluate oil slick boundaries [52].

In the case of intentional spills, two main problems are of concern:

- the detection of illegal oil discharges at sea; and
- the identification of the culprit, which is a task considerably more complicated than the former. As a reference case, the Mediterranean basin scenario will be considered. An important difference from the monitoring of an oil accident is that the location of illegal spills along these routes is not a priori known. Therefore, "blind surveillance" must be performed, taking into consideration the distribution of the tanker routes. The basic technique consists of getting regular updates of maps of the sea surface, possibly in both the IR and radar bands, for comparing, on a daily basis, the newly acquired data with those obtained on the previous days in order to detect the presence of new oil spills and the drift of older ones. The satellite orbit choice should match the orientation of the major traffic paths. Each satellite must be capable of wide swaths, preferably implementing a dual SAR antenna to image sea strips on both sides with respect to the satellite nadir. The SAR instrument could have a resolution around 15 m and a swath width on the order of 150 km. It was shown that by increasing the number of satellites the mean and peak revisit intervals decrease. This leads to a greater chance of timely oil spill detection, better oil slick drift tracking, and ship route determination, and, therefore, increases the probability of identifying the ships responsible for illegal waste according to the methodology discussed in the next paragraph. On the other hand, the number of images generated and processed daily will also increase in proportion, leading to the need for automatic photo-interpretation tools [52].

In addition to the identification and tracking of oil spills, it is also important to identify which ship was responsible for illegal waste. The latter task is very complex because it is necessary to detect and identify a whole variety of ships in transit and to correlate them to the tracked oil spills. There are, nevertheless, certain positive factors to be considered in this effort. For instance, a tanker is much larger than a fishing vessel and thus provides a stronger radar return. Other features can be exploited to discern tankers from other ships, among which the vessel velocity and mean velocity vector direction and the ship's electromagnetic (radar) signature or its IR signature, provided that the data are compared with known databases. Anyway, we will assume that means can be devised to, at least, discern tankers among a population of vessels in a given sea portion. Tanker tracking can be performed by sampling the area around preselected routes at regular intervals. At 15–20 knots cruising speed, a sampling time considerably less than 6 h seems necessary for ships' routes restitution. Data concerning departure time from harbour, of destination and approximate trip-time forecast of tankers in transit, are normally available from harbour authorities and contribute considerably to the identification of the vessels [52].

Following the detection of an oil slick, the use of satellite remote sensing is a powerful tool to support relief operations directed to damage containment or clean-up activities. The "observation variables" most significant during the relief phase are as follows:

- Oil spill size: where remote sensing can provide a synoptic view of large areas and can be used to estimate the dimensions of the spill and to monitor its temporal evolution.
- Thickness and volume evaluation.

- Oil classification: Lidar fluorosensors are used to measure thicknesses less than 10 mm and to discriminate between oil types. Such sensors are not yet readily available for space applications.
- Wind fields: Wind field maps, if available, support oil slick motion predictions and facilitate tracking. At a local level, the scale is too small for space-based measurements; therefore, their operational use is highly questionable.
- Currents speed and direction: Precision altimetry packages and SAR are significant data sources, but at the local level the scale is probably too small for space-based measurements.
- Sea surface temperature: SST data are used to derive marine current characteristics and profiles in order to predict the spill drift. TIR imagers are used for SST measurements; most have spatial resolution and accuracies of the order of 1 km and 0.2–0.7 K, respectively, and are thus compatible with the stated application [52].

However, not all of the above instruments will have the same priority, and it is not necessary for all considered tasks to be performed by spaceborne sensors. Especially in closed sea basins, some of the oil slick classification tasks would be better performed by airborne rather than spaceborne sensors. In addition, many existing satellites already provide information that can be used to support the modeling of marine currents and the assessment of meteorological and environmental conditions. Therefore, a dedicated satellite system should primarily address those tasks that are highly specific to the relief phase, with the greatest emphasis on the measurement of the oil spill extent, shape, and important parameters for oil slick motion tracking. In this context, a SAR satellite constellation, which has the required revisit interval performance and resolution characteristics, is well suited to support relief phase operations. This satellite system may also carry TIR sensors for use in the characterization of sea currents [52].

After this brief overview of oil remote sensing technologies, requirements, advantages, and limitations, some applications and case studies will be mentioned. Efforts to establish operational systems that detect oil spills through SAR images after processing have been reported in the literature [42,52–57].

Three basic requirements have been identified in order to develop an operational oil spill monitoring system based on satellite SAR images: (a) availability of SAR data, (b) fast reaction to alarms, and (c) high reliability of the alarms. It has been reported by Martinez and Moreno, 1996 [44] that in the case of the Spanish coast the reaction time is determined by the ground infrastructure. A serious problem is the delay of acquisition of SAR data, which can be at worst 2 weeks, or at best 24 hours, far from operational requirements. The key requirement is the availability of a data reception station that can provide the data within a few minutes of acquisition. The duration of the data processing steps are important only if the data acquisition problem is solved [42].

Research groups have been analyzing SAR images from several marine areas with increased oil pollution problems. For example, 660 SAR images acquired over the southern Baltic Sea, the North Sea, and the Gulf of Lion in the Mediterranean Sea by the European Remote Sensing Satellite ERS-2 were analyzed since December 1996 with respect to radar signatures of marine pollution and other phenomena causing similar signatures. The first results of the analysis reveal that the seas are most polluted along the main shipping routes. The sizes of the detected oil spills vary between <0.1 km^2 and >56 km^2. SAR images acquired during descending (morning) and ascending (evening) satellite passes show different percentages of oil pollution, because most of this pollution occurs during night time and is still visible on the SAR images acquired in the morning time. Moreover, a higher amount of oil spills on SAR images acquired was found during summer (April–September) than on SAR images acquired during winter (October–March). This was attributed on the higher mean wind speed encountered in all three test areas during winter. Several ERS-2 SAR images showed so-called look-alikes, that is, radar signatures looking similar to those caused by oil pollution. Therefore, it was concluded that for an effective oil spill surveillance system a good understanding is required of radar signatures caused by oceanic and atmospheric phenomena that give rise to similar radar signatures as those by oil spills. Statistical analysis of SAR images should comprise, for example, the consideration of mean wind speed in the particular areas during image acquisition; a better classification of the observed phenomena, particularly of the observed oil pollution; and synoptic studies using optical and microwave data from the other sensors [53].

A research paper described the ongoing efforts at the Nansen Environmental and Remote Sensing Centre (NERSC) to integrate SAR imagery into an operational coastal monitoring system for Norway. The capabilities of the SAR to image ocean waves, internal waves, bathymetry, eddies, fronts, natural film, oil slicks, and wind in the marine boundary layer, have already been demonstrated. In order to quantify products of ocean fronts, natural films, wind speed, and wind fronts, SAR imagery obtained along the southern coast of Norway has been analyzed in conjunction with in situ information, numerical models and other available remote sensing data. The results were used in the process of validation and improvement of SAR ocean models and SAR operational applications [54].

Oil spill pollution is also a serious threat to marine environments along the United Arab Emirates (UAE) coast line. Considerable oil spills have been caused by accidental and deliberate oil sludge dumping from passing ships. The purpose of one study was to investigate and demonstrate the feasibility of using different types of satellite imagery for detecting oil spills in the Arabian Gulf, offshore the UAE. A number of satellite data were processed and analyzed by using images from early U.S. satellites from the mid-1970s to more recent satellites (European ENVISAT, 2003). It was confirmed that the offshore of the UAE faces frequent occurrences of oil spills in the Arabian Gulf and in the Gulf of Oman. Discharged oil and widely spread oil slicks in offshore Fujairah were confirmed by an in situ campaign carried out in early 2003. This work was considered the first step toward oil spill monitoring of the offshore UAE and its adjacent waters, while an ultimate goal would be an operational monitoring system integrating near-real-time satellite observation with GIS mainframe to create an early warning system and protect the marine environment of the Gulf States against oil pollution [55].

In the Eastern Mediterranean there also have been fragmentary research efforts on oil spill monitoring by individual research team with no central design.

A fully automated system for the identification of possible oil spills on SAR satellite images based on artificial intelligence fuzzy logic was also developed by Greek researchers [56]. Oil spills are recognized by experts as dark patterns of characteristic shape, in particular context. The system developed analyzes the satellite images and assigns the probability of a dark image shape to be an oil spill. The output consists of several images and tables, providing the user with all relevant information for decision-making. The case study area was the Aegean Sea in Greece. The system responded very satisfactorily for all 35 images processed.

Case 1: The original SAR image is illustrated in Fig. 20a and is the first visual output of the algorithm. The image is acquired over the island of Milos in Cyclades, Aegean Sea, Greece. The image presents only a small number of dark regions (13 in total) owing to moderate wind conditions. The image with the land masked out is illustrated in Fig. 20b; this is the second visual output in bitmap format. After the thresholding, segmentation, and fuzzy classification processes, the result comes out as a third visual output (Fig. 20c). In this figure, the candidate objects are painted with colours ranging from green to red, showing the probability of the object to be an oil spill: green is low probability (0 %) whilst red is very high probability (100 %). Therefore, when the software is used in an operational mode, the user can immediately depict the areas to be visited for in situ or aerial inspection. The algorithm also generates a tabular output (Table 2), which gives useful information about the scene, such as the number of dark objects around the candidate oil spill, the area of each candidate object (in km^2), the eccentricity and proximity to land as well as its geographic coordinates (latitude and longitude in degrees). The table contains the shape of each coloured dark object according to its probability to be an oil spill. The algorithm depicted correctly the verified oil spill seen at the southeastern corner of the image and assigned to it a probability of 80 % to be an oil spill [56].

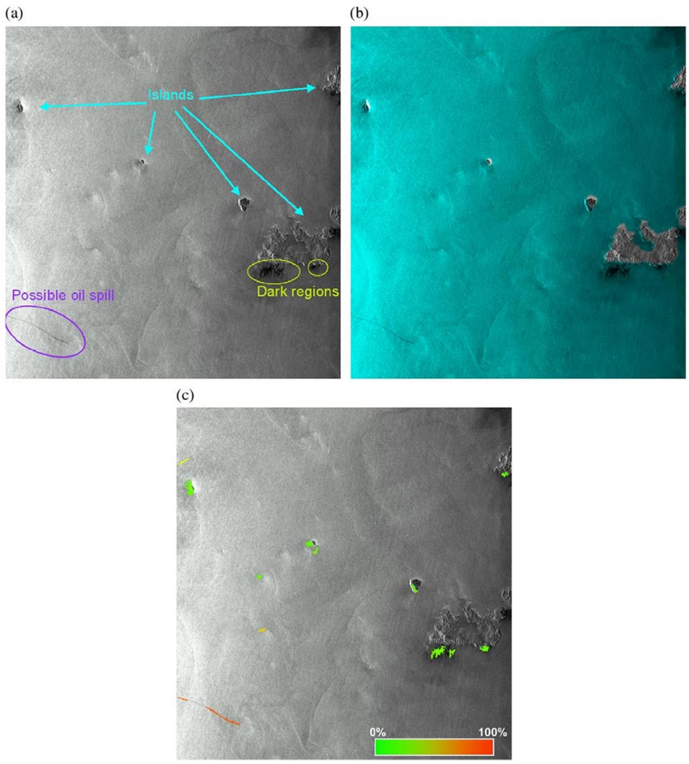

Fig. 20 SAR image with verified oil spill and 13 dark objects adjacent to and between the islands: (a) original scene, (b) land masked image, and (c) output image with dark objects coloured according to their possibility to be oil spills (green is low, red is high).

Table 2 Sample tabular output from scene depicted in Figs. 20a–c.

Dark object on image	Number of objects around	Area (km^2)	Eccentricity	Land distance (km)	Longitude (°N)	Latitude (°E)	Probability to be an oil spill (%)
	1	0.843	9.377	32.718	23.58	36.37	76.509
	1	1.081	5.888	5.214	23.41	36.98	50.000
	1	4.587	2.066	0.883	23.45	36.91	21.541
	1	3.124	15.776	44.716	23.72	36.35	80.686
	0	0.994	1.067	16.418	23.73	36.72	21.614
	0	1.002	2.735	23.127	23.78	36.59	59.317
	1	2.019	1.470	1.210	23.87	36.84	19.356
	1	1.097	2.312	1.093	23.90	36.82	24.809
	0	1.383	4.028	0.449	24.24	36.78	19.681
	1	5.048	2.237	2.418	24.35	36.63	23.087
	2	1.590	1.789	2.189	24.40	36.63	23.387
	2	2.210	1.715	0.655	24.50	36.66	20.093
	0	1.542	1.266	1.072	24.45	37.12	19.485

Case 2: The original SAR image is illustrated in Fig. 21a. The image is acquired over the islands of Milos, Sifnos, Serifos, and Paros in Cyclades, Aegean Sea. The image presents a larger number of dark regions compared to Case 1, especially close and between the islands. The total number of dark objects is 59. The image with the land masked out is illustrated in Fig. 21b; this is the second visual output of the algorithm. The third visual output is presented in Fig. 21c. In this case, the algorithm depicted correctly the low probability of the dark objects adjacent to and in between the islands to be oil spills. These formations are due to local low wind conditions. Furthermore, it assigned a high probability of 78 % to the verified oil spill shown on the northwestern part of the image. A sample of the tabular output corresponding to this case study is given as Table 3 [56].

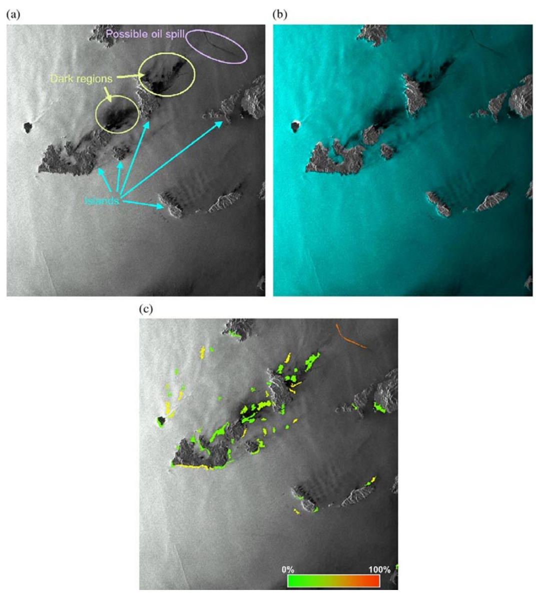

Fig. 21 SAR image with verified oil spill and 59 dark objects.

Table 3 Sample tabular output from scene depicted in Figs. 21a–c.

Dark object on image	Number of objects around	Area (km^2)	Eccentricity	Land distance (km)	Longitude (°N)	Latitude (°E)	Probability to be an oil spill (%)
	2	0.811	2.750	0.081	24.88	36.63	23.107
	9	10.073	2.760	0.342	24.81	37.09	22.707
	2	1.169	2.650	0.357	24.96	36.60	23.10
	2	1.224	10.723	12.583	24.89	37.22	78.389
	2	2.679	20.210	14.792	24.97	37.19	76.606
	1	1.081	3.579	0.143	25.03	36.97	23.440
	1	1.169	2.596	0.311	25.15	36.72	23.187
	1	1.336	2.738	1.937	25.17	36.74	49.080
	1	5.199	2.915	1.057	25.13	36.98	22.460
	0	0.835	2.548	0.632	25.34	36.47	23.148

Case 3: The original SAR image is illustrated in Fig. 22a. The image is acquired east of Peloponissos, northeast of Kithira Island, Aegean Sea. The image presents a very large number of dark regions (117 in total), owing to low wind conditions and no oil spill. Therefore, the dark objects are all look-alikes. The image with the land masked out is illustrated in Fig. 22b. After the thresholding, segmentation, and fuzzy classification processes, the resultant image is presented in Fig. 22c. The algorithm depicted correctly that the probability of these objects to be oil spills is low and has left out the very large dark regions, owing to their size. The corresponding sample tabular output is given in Table 4 [56].

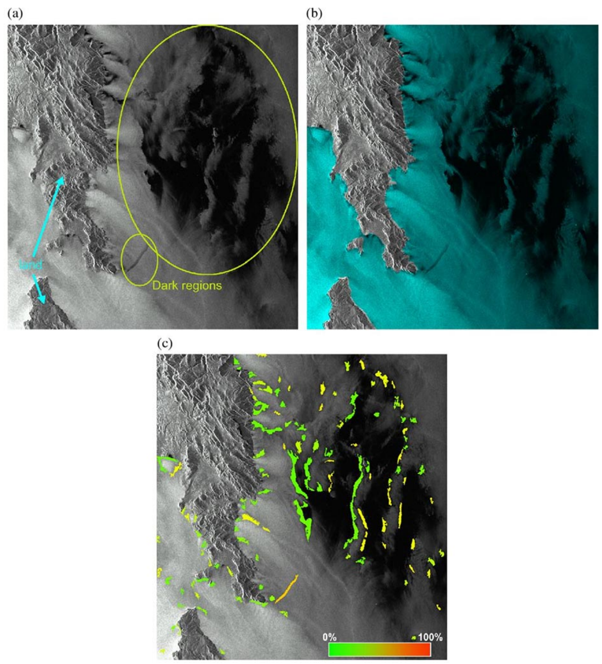

Fig. 22 SAR image containing only look-alikes (117).

Table 4 Sample tabular output from scene depicted in Figs. 22a–c.

Dark object on image	Number of objects around	Area (km^2)	Eccentricity	Land distance (km)	Longitude (°N)	Latitude (°E)	Probability to be an oil spill (%)
	1	7.131	1.175	1.519	22.72	36.79	20.072
	3	1.614	1.867	9.996	22.76	36.56	39.096
	5	2.202	2.570	12.247	22.79	36.47	48.161
	2	0.938	1.237	3.317	22.86	36.23	43.557
	9	2.465	1.845	9.091	22.83	36.45	22.593
	2	4.333	3.546	1.948	22.77	36.78	48.695
	5	1.200	1.588	1.551	22.88	36.31	27.922
	6	1.081	3.762	0.442	22.91	36.31	38.447
	10	1.129	1.843	2.576	22.89	36.38	22.881
	1	1.010	1.630	4.885	22.89	36.42	21.471
	6	1.296	3.356	0.343	22.83	36.66	40.338
	6	1.781	1.866	2.440	22.85	36.64	48.028
	11	1.375	2.196	1.753	22.92	36.45	31.581

Another Greek research team has also analysed Radarsat images from the Aegean Sea. After the appropriate processing and algorithm implementation, the result is the image presented in Fig. 23a. The colour scale is as follows: red – centre of possible oil spill; yellow – one level below the centre of possible oil spill; green – minimum amount of oil; blue – clean sea [57].

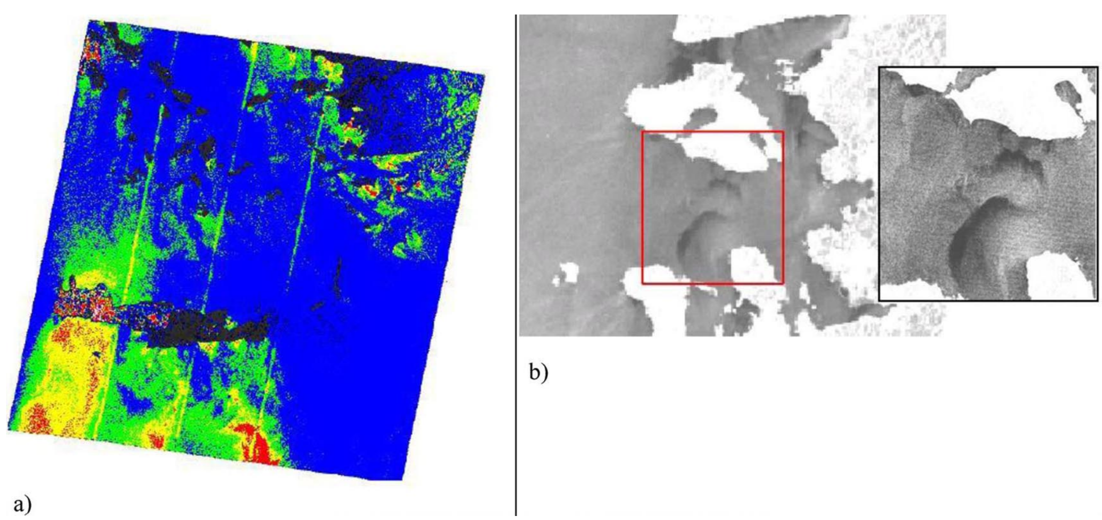

Fig. 23 (a) Processed Radarsat image of the central and south Aegean Sea and (b) processed Radarsat image south of Mytilene Island (Greece). The algorithm generated high probability that the dark images are oil spills [57].

In order that remote sensing may have a successful role in supporting risk and damage reduction of oil spills, as well as ensuring law enforcement efficacy, it should be considered within the concept of a totally integrated marine traffic surveillance system (TIMTSS) that will address all of the above-mentioned issues. A TIMTSS is shown in Fig. 24 and should include the following three basic functional subsystems:

(1) space information and communication system (SICS), consisting of an observation satellite constellation, a telecommunication satellite system, the maritime traffic surveillance integrated management system (MTSIMS), and a meteo satellite system;
(2) conventional information and surveillance system (CISS), consisting of airborne surveillance systems (complementary to satellites and for operational support to field groups), ground surveillance systems, and a maritime intelligence and information system (vessel routes plans and identification information to operations); and
(3) MTSIMS, consisting of a data reception, processing, archiving and distribution system and a maritime traffic surveillance logistics support and training system **(author: check editing)**.

The TIMTSS concept may be implemented at the continental level (e.g., Europe) with regional management subfunctions converging in a common effort. This will permit, for example, the use of common observation constellations for global instead of regional coverage. A TIMTSS could be used to address accidental disasters and surveillance of closed sea basins to detect illegal discharges [52].

Despite the limitations of satellite revisit times in detecting smaller incidents of oil spills, i.e., in the major shipping routes, once an accident has become known satellite images are very useful in monitoring the movement of the spill. This has been proven in the latest accident in the Gulf of Mexico where satellite images of the spill are available on line [58].

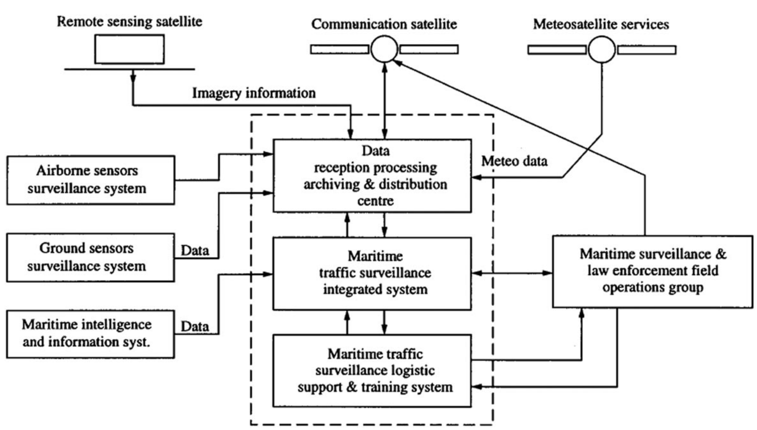

Fig. 24 TIMTSS: main functional block diagram [52].

11. CONCLUSIONS

The ocean ecosystems are threatened by the impacts of chemical pollution, nutrient loading, harvesting of marine resources, and habitat destruction. The alterations in ocean temperature, stratification patterns, bio-geochemistry, and the induced acidification because of change and subsequently are also significant current problems. Management of these threats is critical to sustaining benefits to society for both present and future generations. Observing the oceans is critical to understand, assess, forecast future threats, and manage and reduce human vulnerability and risk linked to the oceans.

Technologies for ocean observations are advancing at a rapid rate. Some new elements of a sustained ocean observing system are ready for immediate implementation and could create new global observing networks. Their implementation will quickly enable new science and new information support tools for a range of decisions. Other elements are emerging and will require additional development in technology or methodology to enable them to contribute to the future sustained ocean observing system.

A future global integrated ocean information system would have to include observations from both satellite and in situ platforms and also a data managing infrastructure based on common standards, analysis. and modeling systems.

Innovation in sensor technology and platforms should be encouraged to expand the capabilities of the system or provide information on environmental processes of the coastal area and the open oceans.

Ships will continue to play a multitude of functions in an integrated observing system as platforms carrying many high-quality instruments. Ships are also important to the testing of new technology. Moorings are platforms that can carry a multitude of sensors for high temporal-resolution observations at key sites, capturing important events with fast data transmission. Expanding the spatial coverage of mooring sites and the suite of sensors deployed could greatly expand the importance of mooring data. The existing Lagrangian buoy networks (the surface drifter array and the subsurface Argo profiling float array) have been a demonstrated success. In both cases, the existing arrays need to be maintained at their initial target densities and for their original design goals, but more sensors could be added.

Satellites are now a central part of the ocean observing system. Satellites observe the ocean globally with high space-time sampling, irrespective of political boundaries, and provide observations year-round, often independent of weather systems and seasons. In the future, it can be expected that hyper-spectral technology will gain increased importance to resolve more processes and phenomena than can be observed with current technology. This will increase the number of bio-geochemical and ecosystems variables that can be inferred.

The extraction of ocean information from satellite measurements in an optimal way requires a merger with in situ data (also required for calibration purposes) through analysis and dynamically consistent synthesis activities. A close link between the satellite community and the data assimilation/modeling community needs to continue for an optimal use of satellite and in situ data.

The real wealth of information, in the case of environmental remote sensing, is to be found in the long-term, large-scale monitoring of interacting bio-geochemical and physical processes. This means that unique opportunities are offered by the capabilities, now being developed, of integrating remote sensing data into value-added realizations of environmental parameters of importance on land, along the shoreline and in the sea. This will allow generation of synoptic, repetitive, statistically significant time series of composite images describing the variations of such parameters in time, over entire basins.

Sensors are at the core of expanding the capabilities of the ocean observing system, as they bring the ability to make stable sustained measurements of new variables. The further improvement of current bio-geochemical sensors and the construction of new ones will be key to developing an integrated observation system across disciplinary boundaries. The development of in situ nutrient sensors allowing real-time data transmission will provide new and important insights into global bio-geochemical cycles. There are also some biological sensors that are currently being introduced or improved for the determination of chl a and particulate organic carbon, which would provide critical bio-optical measurements for the validation of ocean colour remote sensing.

An effective data management system is vital to nearly every element of the ocean observing system. It serves essential functions in the program-level management of in situ platforms and sensors; in the timely and reliable delivery of observations to data assimilation and data assembly centres; in linking observations to the metadata that describes them; in the feedback loops that ensure quality control of observations; and in the creation and delivery of products. It has a highly visible role in meeting the needs of scientists, environmental planners, educators, and many other classes of users, who need to access data and information.

In the case of the Mediterranean Sea, the increased capabilities of remote sensing systems for marine observation and monitoring are not yet used properly and widely. In order to take full advantage of the data devoted to the Mediterranean environment, the following scientific issues should be tackled:

- mapping of runoff patterns, river discharge, and mixing processes, for modeling sediment influx, areas of erosion, zones of long-shore sediment transport, and places of sedimentation;
- water circulation patterns, from major basin-scale currents to smaller mesoscale events in the surface layers, as well as exchanges with deeper layers; and
- monitoring of variations in the concentration and distribution of water constituents in relation to coastal runoff or atmospheric input and water circulation features, the implication of such variations for the cycling of various elements, and possible environmental feedbacks.

The main requirement of oil spill detection and monitoring is the timely acquisition and processing of remotely sensed data, for use in containment and clean-up operations, with a limited delay from the occurrence of the event. Enhanced constellations (provided with a greater number of satellites) can be designed to cope with the more challenging task of identifying tankers responsible for illegal oil spills in closed sea basins, with the aim of supporting law enforcement actions.

Additional effort is needed from the oceanographic scientific community of all Mediterranean countries to increase the use of remote sensing systems in parallel with standard oceanographic cruises in order to increase the knowledge of the total Mediterranean system and improve its management for the success of sustainability.

MEMBERSHIP OF SPONSORING BODY

Membership of the IUPAC Chemistry and the Environment Division Committee for the period 2010–2011 was as follows:

***President*:** N. Senesi (Italy); ***Vice President*:** L. L. McConnell (USA); ***Secretary*:** W. J. G. M. Peijnenburg (Netherlands); ***Titular Members*:** E. M. Cukrowska (South Africa); P. S. Fedotov (Russia); S. H. Herve (Finland); N. G. Kandile (Egypt); W. Kördel (Germany); K. Tanaka (Japan); P. H. Wine (USA); ***Associate Members*:** M. Dassenakis (Greece); H. Garelick (UK); L. Klasinc (Croatia); K. D. Racke (USA); E. Tombácz (Hungary); C. von Holst (Belgium); ***National Representatives*:** M. I. Bhanger (Pakistan); M. E. Goodsite (Denmark); G. Jiang (China); R. Kookana (Australia); N. Mañay (Uruguay); S. Safiullah (Bangladesh); Y. Shevah (Israel); T.-K. Soon (Malaysia); S. Tepavitcharova (Bulgaria); M. Veber (Slovenia); P. Visoottiviseth (Thailand).

REFERENCES

1. Natural Resources Canada. *Tutorial: Fundamentals of Remote Sensing*, <http://www.ccrs.nrcan.gc.ca/resource/tutor/fundam/index_e.php>, modified 25 September 2007.
2. Committee on Earth Observation Satellites. *The Earth Observation Handbook: Catalogue of Satellite Missions*, <http://database.eohandbook.com/database/missiontable.aspx>, accessed 5 April 2010.
3. I. Joint, S. B. Groom. *J. Exper. Mar. Biol. Ecol.* **250**, 233 (2000).
4. NASA. MODUS Atmosphere, <http://modis-atmos.gsfc.nasa.gov/>, accessed 5 April 2010.
5. European Space Agency. Envisat History, <http://envisat.esa.int/earth/www/category/index.cfm?fcategoryid=87>, accessed 5 April 2010.
6. European Space Agency. Envisat Applications, <http://envisat.esa.int/earth/www/category/index.cfm?fcategoryid=88>, accessed 5 April 2010.

7. European Space Agency. Envisat MERIS, <http://envisat.esa.int/instruments/meris/>, accessed 5 April 2010.
8. NASA. Aquarius: Sea Surface Salinity from Space, <http://aquarius.nasa.gov/overview-mission.html>, accessed 5 April 2010.
9. A. I. Ginzburg, A. G. Kostianoy, N. A. Sheremet. *J. Mar. Syst.* **52**, 33 (2004).
10. S. Marullo, R. Santoleri, P. Malanotte-Rizzoli, A. Bergamasco. *J. Mar. Syst.* **20**, 63 (1999).
11. S. Marullo, R. Santoleri, P. Malanotte-Rizzoli, A. Bergamasco. *J. Mar. Syst.* **20**, 83 (1999).
12. N. Hamad, C. Millot, I. Taupier-Letage. *Prog. Oceanogr.* **66**, 287 (2005).
13. G. Larnicol, N. Ayoub, P. Y. Le Traon. *J. Mar. Syst.* **33–34**, 63 (2002).
14. J. Salas, C. Millot, J. Font, E. Garcıa-Ladona. *Deep-Sea Res. I* **49**, 245 (2002).
15. J. Isern-Fontanet, J. Font, E. Garcia-Ladona, M. Emelianov, C. Millot, I. Taupier-Letag. *Deep Res. II* **51**, 3009 (2004).
16. A. Rubio, P. A. Arnau, M. Espino, M. del Mar Flexas, G. Jorda, J. Salat, J. Puigdefabregas, A. Arcilla. *Prog. Oceanogr.* **66**, 142 (2005).
17. V. Barale, S. Folving. *Rem. Ocean Coast. Manag*. **30**, 217 (1996).
18. V. Barale, J. M. Jaquet, M. Ndiaye. *Rem. Sens. Environ.* **112**, 3300 (2008).
19. C. R. McClain, G. C. Feldman, S. B. Hooker. *Deep-Sea Res. II* **51**, 5 (2004).
20. S. W. Bailey, C. R. McClain, P. J. Werdell, B. D. Schieber. In *SeaWiFS Postlaunch Calibration and Validation Analyses: Part 2*, Vol. 10, C. R. McClain, S. B. Hooker, E. R. Firestone (Eds.), pp. 45–52, NASA Tech. Memo. 2000-206892, Greenbelt (2000).
21. J. E. Reilly, S. Maritorena, D. A. Siegel, M. C. O'Brien, D. Toole, B. G. Mitchell, M. Kahru, F. P. Chavez, P. Strutton, G. F. Cotta, S. B. Hooker, C. R. McClain, K. L. Carder, F. Moller-Karger, L. Harding, A. Magnuson, D. Phinney, G. F. Moore, J. Aiken, K. R. Arrigo, R. Letelier, M. Culver. In *SeaWiFS Postlaunch Calibration and Validation Analyses: Part 3*, Vol. 11, S. B. Hooker, E. R. Firestone (Eds.), pp. 9–23, NASA Tech. Memo. 2000-206892, Greenbelt (2000).
22. G. Volpe, R. Santoleri, V. Vellucci, M. Ribera d'Alcalà, S. Marullo, F. D'Ortenzio. *Rem. Sens. Environ*. **107**, 625 (2007).
23. S. Groom, B. Herut, S. Brenner, G. Zodiatis, S. Psarra, N. Kress, M. D. Krom, C. S. Law, P. Drakopoulos. *Deep-Sea Res. II* **52**, 2990 (2005).
24. A. Bricaud, E. Bosc, D. Antoine. *Rem. Sens. Environ*. **81**, 163 (2002).
25. N. Kabbaraa, J. Benkhelil, M. Awad, V. Barale. *ISPRS J. Photogr. Rem. Sens.* **63**, 488 (2008).
26. A. Goufa. Academic Dissertation, University of Aegean, School of the Environment, Department of Environmental Studies (in Greek only) (1994).
27. B. Herut, G. Tibor, Y. Z. Yacobi, N. Kress. *Mar. Polut. Bull.* **38**, 762 (1999).
28. A. Nair, S. Sathyendranath, T. Platt, J. Morales, V. Stuart, M. Forget, E. Devred, H. Bouman. *Rem. Sens. Environ*. **112**, 3366 (2008).
29. T. Hirata, J. Aiken, N. Hardman-Mountford, T. J. Smyth, R. G. Barlow. *Rem. Sens. Environ.* **112**, 3153 (2008).
30. T. K. Alexandridis, E. Lazaridou, A. Tsirika, G. Zalidis. *J. Environ. Manag.* **90**, 2243 (2009).
31. K. White, H. M. El Asmar. *Geomorphology* **29**, 93 (1999).
32. H. M. El Asmar, K. White. *Coast. Eng*. **46**, 127 (2002).
33. A. Masoud, K. Koike. *J. Afr. Earth Sci.* **45**, 467 (2006).
34. Ph. Paillou, M. Schuster, S. Tooth, T. Farr, A. Rosenqvist, S. Lopez, J.-M. Malezieux. *Earth Planet. Sci. Lett.* **277**, 327 (2009).
35. M. Kouli, K. St. Seymour. *Geomorphology* **77**, 1 (2006).
36. A. Fornes, G. Basterretxea, A. Orfila, A. Jordi, A. Alvarez, J. Tintore. *ISPRS J. Photogr. Rem. Sens*. **60**, 315 (2006).
37. V. Pasqualini, C. Pergent-Martini, G. Pergent, M. Agreil, G. Skoufas, L. Sourbes, A. Tsirika. *Rem. Sens. Environ*. **94**, 39 (2005).

38. D. E. Raitsos, G. Beaugrand, D. Georgopoulos, A. Zenetos, M. A. Pancucci-Papadopoulou, A. Theocharis, E. Papathanassiou. *Limnol. Oceanogr.* **55**, 1478 (2010).
39. S. Panigada, M. Zanardelli, M. MacKenzie, C. Donovan, F. Mélin, P. S. Hammond. *Rem. Sens. Environ.* **112**, 3400 (2008).
40. A. Littaye, A. Gannier, S. Laran, J. P. F. Wilson. *Rem. Sens. Environ.* **90**, 44 (2004).
41. R. Goodman. *Spill Sci. Technol. Bull.* **1**, 11 (1994).
42. A. Martinez, V. Moreno. *Spill Sci. Technol. Bull.* **3**, 65 (1996).
43. M. F. Fingas, C. E. Brown. *Spill Sci. Technol. Bull.* **4**, 199 (1997).
44. C. Brekke, A. H. S. Solberg. *Rem. Sens. Environ.* **95**, 1 (2005).
45. L. De Domenico, E. Crisafi, G. Magazzu, A. Puglisi, A. La Rosa. *Mar. Pollut. Bull.* **28**, 587 (1994).
46. M. Indregard, A. Solberg, P. Clayton. Tech. rep., Oceanides project, European Commission, Archive No. 04-10225-A-Doc (2004).
47. K. W. Bjerde, A. H. S. Solberg, R. Solberg. *Proc. IGARSS'93* **3**, 943 (1993).
48. A. H. S. Solberg, R. Solberg. *Proc. IGARSS'96* **3**, 1484 (1996).
49. A. H. S. Solberg, E. Volden. *Proc. IGARSS'97* **1**, 157 (1997).
50. A. H. S. Solberg, G. Storvik, R. Solberg, E. Volden. *IEEE Trans. Geosci. Rem. Sens.* **37**, 1916 (1999).
51. A. H. S. Solberg, S. T. Dokken, R. Solberg. *Proc. IGARSS'03* **3**, 2747 (2003).
52. G. Perrrotta, P. Xefteris. *Spill Sci. Technol. Bull.* **3**, 73 (1996).
53. M. Gade, W. Alpers. *Sci. Total Environ.* **237–238**, 441 (1999).
54. O. M. Johannessen, H. A. Espedal, B. Furevik, D. Akimov, A. Jenkins. *Els. Ocean. Ser.* **66**, 455 (2002).
55. S. Essa, H. Harahsheh, M. Shiobara, T. Nishidai. *Dev. Earth Environ. Sci.* **3**, 31 (2005).
56. I. Keramitsoglou, C. Cartalis, C. T. Kiranoudis. *Environ. Model. Soft.* **21**, 640 (2006).
57. K. Topouzelis. Academic dissertation, University of Aegean, School of the Environment, Department of Environmental Studies (in Greek only) (1999).
58. NASA. Imagery of Oil Spill, <http://www.nasa.gov/topics/earth/features/oilspill/index.html>, accessed 15 July 2010.
